AMERICAN SOCIETY FOR MICROBIOLOGY | Molecular and Cellular Biology

The Poly(C) Binding Protein Pcbp2 and Its Retrotransposed Derivative Pcbp1 Are Independently Essential to Mouse Development

Louis R. Ghanem,[a,b] Andrew Kromer,[b] Ian M. Silverman,[b] Priya Chatterji,[b] Elizabeth Traxler,[c] Alfredo Penzo-Mendez,[d] Mitchell J. Weiss,[e] Ben Z. Stanger,[d] Stephen A. Liebhaber[b,f]

Gastroenterology, Hepatology and Nutrition Division, The Children's Hospital of Philadelphia, Philadelphia, Pennsylvania, USA[a]; Department of Genetics, Perelman School of Medicine at the University of Pennsylvania, Philadelphia, Pennsylvania, USA[b]; Cell and Molecular Biology Graduate Group, Perelman School of Medicine at the University of Pennsylvania, Philadelphia, Pennsylvania, USA[c]; Gastroenterology Division, Department of Medicine, Perelman School of Medicine at the University of Pennsylvania, University of Pennsylvania, Philadelphia, Pennsylvania, USA[d]; Department of Hematology, St. Jude Children's Research Hospital, Memphis, Tennessee, USA[e]; Division of Hematology and Oncology, Department of Medicine, Perelman School of Medicine at the University of Pennsylvania, Philadelphia, Pennsylvania, USA[f]

RNA-binding proteins participate in a complex array of posttranscriptional controls essential to cell type specification and somatic development. Despite their detailed biochemical characterizations, the degree to which each RNA-binding protein impacts mammalian embryonic development remains incompletely defined, and the level of functional redundancy among subsets of these proteins remains open to question. The poly(C) binding proteins, PCBPs (αCPs and hnRNP E proteins), are encoded by a highly conserved and broadly expressed gene family. The two major Pcbp isoforms, Pcbp2 and Pcbp1, are robustly expressed in a wide range of tissues and exert both nuclear and cytoplasmic controls over gene expression. Here, we report that *Pcbp1*-null embryos are rendered nonviable in the peri-implantation stage. In contrast, *Pcbp2*-null embryos undergo normal development until midgestation (12.5 to 13.5 days postcoitum), at which time they undergo a dramatic loss in viability associated with combined cardiovascular and hematopoietic abnormalities. Mice heterozygous for either Pcbp1 or Pcbp2 null alleles display a mild and nondisruptive defect in initial postpartum weight gain. These data reveal that *Pcbp1* and *Pcbp2* are individually essential for mouse embryonic development and have distinct impacts on embryonic viability and that Pcpb2 has a nonredundant *in vivo* role in hematopoiesis. These data further provide direct evidence that *Pcbp1*, a retrotransposed derivative of *Pcpb2*, has evolved an essential function(s) in the mammalian genome.

Posttranscriptional control of gene expression plays a major role in eukaryotic cell type specification and organism development. RNA processing and mRNA expression are regulated in the nuclear and cytoplasmic compartments by a complex array of interactions among RNA-binding proteins, noncoding RNAs, and target transcripts (1, 2). Studies have documented the central importance of posttranscriptional controls in the programming of embryonic stem cell differentiation and somatic cell development (3–11). The critical role of posttranscriptional control of gene expression can be most clearly recognized in settings of transcriptional inactivity. For example, transcription is globally silenced in the differentiating erythroblast, and the terminal steps in erythrocyte formation are fully dependent on posttranscriptional controls over mRNA stability and translation (12–14). Studies of posttranscriptional controls in this and other models have relied heavily upon a variety of *in vitro* experimental platforms to define mechanisms and biochemical pathways. While highly informative, such studies do not address the *in vivo* relevance and nonredundant functions of RNA-binding proteins in physiologically intact environments.

The PCBPs (also known as αCPs and heterogeneous ribonucleoprotein [hnRNP] E proteins) are a widely expressed and multifunctional family of RNA-binding proteins (15–19) that bind numerous erythroid and nonerythroid mRNAs (20, 21). Studies focused on globin gene expression have revealed that the PCBPs can integrate nuclear controls over splicing and 3′ processing with cytoplasmic controls over mRNA stabilization via direct interactions of the PCBPs with cytosine-rich motifs in target RNAs (22–25). Transcriptome-wide analyses reveal that PCBPs have an impact on the structure, abundance, and function of RNAs encoded by multiple gene subsets throughout the mammalian transcriptome (20, 26).

PCBPs are encoded by four dispersed loci, *Pcbp1* to *Pcbp4* (15, 16, 25). The ubiquitous expression profiles of the major isoforms Pcbp1 and Pcbp2 contrast with lower and more restricted expression of Pcbp3 and Pcbp4 (27). Alternative splicing of Pcbp2 generates two abundant isoforms, Pcbp2 and Pcbp2-KL. In contrast, *Pcbp 1* is an intronless gene that evolved by retrotransposition of a fully processed Pcbp2 transcript (16). The remarkably high level of structural conservation between PCBP homologues across eukaryotic taxa (15) suggests corresponding constraints in their functions. Perturbation of PCBP paralogs in the invertebrate model organisms *Drosophila melanogaster* and *Caenorhabditis elegans* results in deranged axial patterning, meiotic defects, and lethal phenotypes (28–30). These observations suggest that the Pcbp1 and Pcbp2 genes each serve essential cellular functions.

Received 13 October 2015 **Returned for modification** 27 October 2015
Accepted 28 October 2015

Accepted manuscript posted online 2 November 2015

Citation Ghanem LR, Kromer A, Silverman IM, Chatterji P, Traxler E, Penzo-Mendez A, Weiss MJ, Stanger BZ, Liebhaber SA. 2016. The poly(C) binding protein Pcbp2 and its retrotransposed derivative Pcbp1 are independently essential to mouse development. Mol Cell Biol 36:304–319. doi:10.1128/MCB.00936-15.

Address correspondence to Stephen A. Liebhaber, liebhabe@mail.med.upenn.edu.

Supplemental material for this article may be found at http://dx.doi.org/10.1128/MCB.00936-15.

TABLE 1 Primary antibodies used in this study

Antibody[a]	Source (catalog no.)	Dilution (use)[b]	Host (antibody type)[c]
Pcbp1	Abcam (AB168378)	1:250 (WB)	Rabbit (M)
Pcbp2	Liebhaber laboratory, Philadelphia, PA	1:1,000 (WB)	Rabbit (P)
Gapdh	Pierce (MA5-15738)	1:5,000 (WB)	Mouse (M)
PE-Ter119	BD Biosciences (553673)	1:100 (FACS)	Mouse (M)
APC-CD71	Affymetrix eBioscience (17-0711-82)	1:100 (FACS)	Rat (M)
APC-CD41	Affymetrix eBioscience (17-0411-80)	1:100 (FACS)	Rat (M)
PE-Gr1	Affymetrix eBioscience (12-5931)	1:400 (FACS)	Rat (M)
APC-Mac1	Affymetrix eBioscience (17-0112-83)	1:200 (FACS)	Rat (M)
vWF	Dako (A0082)	1:1,000 (IHC/DAB)	Rabbit (P)

[a] PE, phycoerythrin; APC, allophycocyanin.
[b] WB, Western blotting; FACS, fluorescence-activated cell sorting; IHC, immunohistochemistry; DAB, 3,3′-diaminobenzidine.
[c] M, monoclonal; P, polyclonal.

While several studies have defined critical functions for a number of heterogeneous ribonucleoproteins (hnRNPs) during mammalian embryogenesis, (31–34), the consequences of targeted deletion of Pcbp isoforms upon mouse development and early erythropoiesis remain to be determined.

Pcbp1 and Pcbp2 share a remarkable evolutionary conservation in their structures and in their shared preference for binding C-rich motifs (24). This conservation of structure and of binding specificity is paralleled by sets of shared functions that include control over globin gene expression, viral replication, and cell proliferation (15, 35, 36). More recent work has documented a role for both proteins in intracellular iron transport and as sensors of folate deficiency (37, 38). Importantly, current evidence also suggests that these proteins may have acquired a subset of nonredundant functions. For example, unique functions of Pcbp2 have been demonstrated in HIV gene expression, poliovirus translation, and tumor suppressor gene expression in chronic myelogenous leukemia (39–41). Mechanistic support for Pcbp1-specific functions in development and in response to physiologic stimuli comes from studies of epithelial-mesenchymal transitions (EMT) in secretory epithelium where Pcbp1 has been demonstrated to regulate translational silencing of EMT genes in response to transforming growth factor β (TGF-β) signaling (42, 43). To date, mapping of these isoform-specific functions to discrete domains within either protein has not been demonstrated.

The current study was initiated to determine the *in vivo* impact of the major Pcbp isoforms upon mammalian development and to specifically assess their effects on hematopoiesis in the intact organism. Here, we demonstrate that both Pcbp1 and Pcbp2 have critical and nonredundant functions that are required for fetal survival and normal murine embryogenesis. Importantly, these studies further reveal an essential role for Pcbp2 in erythrocyte and megakaryocyte gene expression and differentiation and in cardiovascular development. These data support the hypothesis that preservation of Pcbp1 over a substantial evolutionary period reflects the evolution of an essential function(s) distinct from the originating Pcbp2 gene.

MATERIALS AND METHODS

Antibodies. Rabbit polyclonal antibodies targeting human Pcbp2 (residues 237 to 251, AIPQPDLTKLHQLAM) (GenBank accession number NP_005007; UniProt accession number Q15366) were generated as previously described (44). Primary antibodies and working dilutions utilized in this study are listed in Table 1. Fluorophore-conjugated secondary antibodies were used for quantitative Western blotting and flow cytometry.

Animals. All experiments were conducted in accordance with protocols approved by the Institutional Animal Care and Use Committee at the Perelman School of Medicine at the University of Pennsylvania. All mice were housed in standard cages within a barrier facility under 12-h on/off light cycling conditions and were given *ad libitum* access to standard mouse chow and water. Euthanasia was achieved by an approved protocol of carbon dioxide inhalation followed by cervical dislocation.

Targeted gene deletion of mouse *Pcbp1* using TALEN endonucleases. For nuclease expression, transcription activator-like effector nuclease (TALEN) expression plasmids (TALEN Sure KO) targeting the mouse *Pcbp1* locus were obtained from Cellectis Bioresearch. The left TALEN (pTAL.CMV.T7.014831) was designed to target chromosome (Chr) 6 coordinates 86525904 to 86525920 (TCGCCATGGACGCCGGT; *Mus musculus* genomic assembly mm10), which encompasses the start codon (underlined). The right TALEN (pTAL.CMV-T7.014862) recognition site, Chr 6 coordinates 86525873 to 86525889 (ACTCAACGTGACT CTCA), was situated 14 bp downstream of the left TALEN targeting sequence. The genomic target sequences and amino acid sequences of the TALEN repeat-variable diresidue (RVD) domains are specified in Table 2. Left and right TALEN mRNAs were each synthesized from 1 μg of plasmid DNA using a mMessage mMachine T7 Ultra kit (catalog number AM1345; Ambion) according to the manufacturer's instructions. Capped and polyadenylated mRNAs were purified using a Qiagen RNeasy kit (74104; Qiagen) and eluted with nuclease-free water. Each TALEN mRNA was diluted to 25 ng/μl in microinjection buffer (10 mM Tris-HCl, pH 7.4, 0.1 mM EDTA). The mRNAs were mixed 1:1 to a final concentration of 50 ng/μl and stored at −80°C until microinjection. Cytoplasmic microinjection was performed in single-cell embryos derived from mating male and female C57BL/6 mice (stock number 000664; Jackson Laboratory, Bar Harbor, ME) at the Transgenic and Chimeric Mouse Facility of the University of Pennsylvania. Embryos were transferred into pseudopregnant CD-1 females (Charles River Production), and resultant pups

TABLE 2 Plasmids used in this study

Plasmid	Target sequence	Repeat-variable diresidue amino acid sequence
pTAL.CMV.T7.014831	TCGCCATGGACGCCGGT	HD-NN-HD-HD-NI-NG-NN-NN-NI-HD-NN-HD-HD-NN-NN-NG
pTAL.CMV.T7.014862	ACTCAACGTGACTCTCA	NN-NI-NN-NI-NN-NG-HD-NI-HD-NN-NG-NG-NN-NI-NN-NG

were screened for mutations by Sanger sequencing of PCR products (forward primer, CGGGGTCAGAGGGTACGCGG; reverse primer, CAGCC GAAGTGTGACCGGGG). PCR products were subcloned using a Zero Blunt PCR TOPO kit (K2830-20; Invitrogen). A minimum of 12 clones were sequenced for each pup. Mouse lines heterozygous for two independent Pcbp1-null alleles were established and designated Pcbp1$^{+/em2}$ and Pcbp1$^{+/em6}$ (see Fig. 2A). The mice in these lines were normal in gross appearance and fertility.

The TALEN recognition elements were screened for potential off-target sites by *in silico* PCR using electronic PCR (e-PCR) and Primer-BLAST tools on the *Mus musculus* genome reference assembly (45, 46). Because TALEN endonuclease activity requires close proximity of the Fok1 nuclease domains to allow for dimerization and optimal cleavage (<30 bp between TALEN recognition sites) (47), we defined conservative search criteria in the e-PCR tool to allow for up to 1,000 bp between two putative off-target sites and up to two mismatches and/or up to 2-bp gaps in each TALEN recognition sequence. The Primer-BLAST algorithm (45) was used to conduct an independent *in silico* off-targeting analysis and was set to the default primer pair specificity checking parameters for the TALEN binding sequences and the *Mus musculus* genome reference assembly.

Derivation of the murine *Pcbp2*-null allele by homologous recombination in embryonic stem (ES) cells. Synthesis of the *Pcbp2* targeting vector was accomplished using previously described recombineering methodology (48). The *Pcbp2* genomic region containing the promoter and exons 1 to 5 was retrieved by gap repair from bacterial artificial chromosome RP23-301N23 (BACPAC Resource Center, Children's Hospital Oakland Research Institute [CHORI], Oakland, CA). The 5′ and 3′ homology arms used for retrieval corresponded to Chr 15 coordinates 102465508 to 102465902 and Chr 15 coordinates 102475270 to 102475653 (*Mus musculus* genomic assembly mm10), respectively. A simian virus 40 polyadenylation (SV40pA) transcriptional termination sequence and *loxP* site were inserted upstream of the Pcbp2 promoter at Chr 15 coordinates 102469582 to 102469583. This 3′ processing signal was included in the targeted locus to block spurious transcriptional read-through from an active upstream locus (Prr13 gene). A neomycin selection cassette and *loxP* site were inserted into intron 2 (*frt-neo-frt-loxP*) by recombineering at Chr 15 coordinates 102473851 to 102473853. The engineered mutant allele resulted in the positioning of *loxP* sequences flanking the 5′ end of the gene and exon 2 (promoter and exons 1 and 2 [exon 2 contains the start codon]). Sequence integrity of the gene-targeting vector was verified by Sanger sequencing.

C57BL/6 × 129/Sv (V6.5) embryonic stem cells (49) (Open Biosystems) were electroporated with the linearized targeting vector according to standard procedures (50). Recombinant clones were selected with G418 (200 μg/ml) and ganciclovir (2 nM). Correct targeting was confirmed by PCR using primers situated on genomic DNA outside the targeting vector footprint paired with primers inside the SV40pA sequence and inside the drug selection cassette. Sanger sequencing of PCR products verified the SV40pA sequence and the junctions between the endogenous locus and gene-targeting cassette. ES cell clones carrying the mutant locus were karyotyped to confirm proper chromosome number. The injected ES clone(s) contained 90.5% cells with normal karyotypes and was mycoplasma negative. Chimeric mice were generated by microinjection of recombinant ES cells into BALB/c blastocysts at the Transgenic and Chimeric Mouse Facility. Male germ line chimeras (Pcbp2$^{+/flox}$) were backcrossed once to female C57BL/6J mice (stock number 000664; Jackson Laboratory, Bar Harbor, ME). To selectively remove the neomycin selection cassette, offspring were crossed to Flp mice [stock number 003946, strain 129S4/SvJaeSor-Gt(ROSA)26Sortm1(FLP1)Dym/J; Jackson Laboratory, Bar Harbor, ME]. To generate the null allele, F1 hybrids were crossed to EIIa-Cre mice [stock number 003724, strain B6.FVB-Tg(EIIa-cre)C5379Lmgd/J; Jackson Laboratory, Bar Harbor, ME]. Offspring carrying the null allele were identified by multiplex PCR (G1 forward [For], ACCTGCATGTGCCTCGGACT; G1 reverse [Rev], GCATC TTACCTCCTCGCGCAT; 5′ Rev, GTACTCTGTGGCCAAGCACA). Thermocycling was performed with a KAPA2G Robust Hot Start PCR kit (KK5518; Kapa Biosystems, Wilmington, MA), as follows: 95°C for 3 min, followed by 35 cycles of 95°C for 30 s, 62°C for 30 s, and 72°C for 80 s, with a final step at 72°C for 3 min. The resultant amplicons defined the mutant allele at 1,214 bp and the wild-type allele at 697 bp. Males carrying the null allele were backcrossed to wild-type female C57BL/6J mice for at least three generations prior to experimentation. Mice heterozygous for the null allele were designated Pcbp2$^{+/-}$.

Tissue fixation and histology. Gestational dating was verified by crown-rump measurements done *ex vivo* at the time of embryo harvest. Embryo macrophotography was done on embryos submerged in ice-cold phosphate-buffered saline (PBS) using a Nikon SMZ-U dissecting microscope and Nikon Coolpix 5000 camera. Dissected embryos were fixed in 4% paraformaldehyde solution (catalog number 19943; Affymetrix) for 24 to 36 h at room temperature, washed once in PBS, and dehydrated in 70% ethanol until paraffin embedding. Subsequent studies utilized 5- to 8-μm sections. For immunohistochemistry, deparaffinized samples were washed in water and heated to 121°C in a pressure cooker for 20 min in 10 mM sodium citrate, pH 6.0, for antigen retrieval. Specimens were extensively rinsed in water, equilibrated with PBS, washed with 3% hydrogen peroxide, and blocked (avidin D and biotin blocking reagents at 2 mg/liter and CAS-Block [00-8120; Invitrogen]). Specimens were incubated with primary antibody (von Willebrand factor [vWF]) (Table 1) overnight at 4°C, washed, and then incubated with biotin-conjugated secondary antibodies (dilution, 1:200). Signals were developed with a 3,3′-diaminobenzidine (DAB) substrate kit per the manufacturer's protocol (Vectastain Elite ABC kit, PK-6100; DAB peroxidase substrate kit, SK-4100; Vector Laboratories).

Flow cytometry. Hematopoietic cells were isolated from 12.5-day postcoitum (dpc) fetal mouse livers. All embryos utilized were visually confirmed to have heartbeats and be morphologically intact at the time of harvest. Livers were dissected and immediately placed into ice-cold PBS supplemented with 2% fetal bovine serum, 2.5 mM EDTA, and 1% penicillin-streptomycin. Single-cell suspensions were generated by gentle pipetting and passage through prechilled cell strainers (catalog number 352235; BD Falcon). After samples were washed with supplemented PBS, cells were resuspended in PBS with antibody (Table 1). A minimum of 30,000 cells per sample were captured on an LSR Fortessa flow cytometer (BD Biosciences), and data were analyzed using FlowJo software in the Flow Cytometry Core Laboratory of The Children's Hospital of Philadelphia Research Institute. The "S staging" system for erythroid differentiation and maturation (stages S0 through S4/5) was used to define gates for quantitation of erythroid progenitors as described previously (51, 52).

qPCR. Fetal tissues for at least three embryos per genotype were obtained from CO_2-euthanized dams. Embryos were kept in ice-cold 1× PBS during dissection. Tissues were immediately excised and homogenized by mortar and pestle in TRIzol reagent (catalog number 15596-018; Invitrogen) at room temperature. All RNA extractions were completed using TRIzol reagent according to the manufacturer's instructions. RNA was resuspended in nuclease-free diethyl pyrocarbonate (DEPC)-treated water (BP5611; Fisher) and quantified by a NanoDrop instrument (model 2000; Thermo Scientific,). One microgram of total RNA was DNase I treated (18068-015; Invitrogen) per the manufacturer's instructions and used for cDNA synthesis. DNase-treated RNA was primed with oligo(dT)$_{12–18}$ (18418-012; Invitrogen) and random hexamers (11034731001; Roche) in the presence of 40 units of RNasin (N2515; Promega) and reverse transcribed for 45 min at 50°C per the vendor's protocol (Superscript III, 200 units/20 μl reaction mixture [18080-044; Invitrogen]). cDNA was diluted 5-fold, and 2.5 μl of diluted cDNA was used for each 20-μl quantitative PCR (qPCR) (Fast SYBR Green mix, catalog number 4385612; Applied Biosystems). qPCR target genes and primer sequences are detailed in Table 3. All primer and amplicon sequences were validated for specificity by a BLAST search against current mouse genomic and RefSeq data sets (45, 53). Synthesized primers were purified by standard desalting spin columns. Thermocycling was per-

TABLE 3 Target genes and primer sequences

Gene symbol	GenBank accession no.	Primer orientation	Primer sequence	Amplicon size (bp)
Alas2	NM_001102446.1	For	TATGTGCAGGCCATCAACTACCCA	94
		Rev	TTTCCATCATCTGAGGGCTGTGGT	
Cebpa	NM_001287514.1	For	CAGACCAGAAAGCTGAGTTGTGA	74
		Rev	ACCCCACAAAGCCCAGAAAC	
Csf2ra	NM_009970.2	For	GTCATGAAGCGATGCTGATAGA	104
		Rev	ACGCCCACTTTGGTGATT	
Gapdh	NM_008084	For	CCTCGTCCCGTAGACAAAATG	124
		Rev	TGAAGGGGTCGTTGATGGC	
Gypa	NM_010369.3	For	TCACACGGCCCCTACTGAAGTGT	149
		Rev	TTCCGATAATCCCTGCCATCACG	
Hba-a1	NM_008218.2	For	CCTGGAAAGGATGTTTGCTAGCT	70
		Rev	GCCGTGGCTTACATCAAAGTG	
Hbb-b1	NM_001278161.1	For	AACGATGGCCTGAATCACTTG	101
		Rev	AGCCTGAAGTTCTCAGGATCC	
Klf1	NM_010635.2	For	CACGCACACGGGAGAGAAG	79
		Rev	CGTCAGTTCGTCTGAGCGAG	
Mpo	NM_010824.2	For	GATCATCACATACCGGGACTAC	99
		Rev	GGGTCTACTGAGTCGTTGTAAG	
Pcbp1	NM_011865.3	For	AATCAATGCCAGGCTTTCCTC	132
		Rev	TTAAAACCTGGAATTACCGACCAG	
Pcbp2	NM_001103165, NM_011042, NM_001103166, NM_001174073	For	AATCAATGCCAGGCTTTCCTC	137
		Rev	TTAAAACCTGGAATCGCTGACTG	
Pf4	NM_019932.4	For	TTCTGGGCCTGTTGTTTCTG	72
		Rev	GATCTCCATCGCTTTCTTCG	
Ppbp	NM_023785.2	For	GCGCAGTTCGATATATGGGT	98
		Rev	ACCTCCAGATCTTGCTGCTG	
Pp1a	NM_008907	For	GCGGCAGGTCCATCTACG	152
		Rev	GCCATCCAGCCATTCAGTC	
Rps29	NM_009093.1	For	TCTACTGGAGTCACCCACGGAA	114
		Rev	GGAAGCACTGGCGGCACA	
Thbs1	NM_011580.4	For	TAGCTGAGGCGGATCAGCAAATCT	112
		Rev	GGGAAGCCAAAGGAGTCCAAATCA	
Vwf	NM_011708.4	For	TCATCGCTCCAGCCACATTCCATA	189
		Rev	AGCCACGCTCACAGTGGTTATACA	

formed on an Applied Biosystems 7900HT Fast real-time PCR system for each primer pair as follows: 95°C for 20 s and then 40 cycles of 95°C for 3 s and 60°C for 30 s. A melt curve analysis was performed at the end of each qPCR run, and single dissociation peaks were verified for all primer pairs. As additional verification, all primer pairs were noted to generate single amplicons of the expected sizes by agarose gel electrophoresis (data not shown). PCR efficiency for all primer pairs was determined by a calibration curve (quantification cycles [*Cq*] versus log fold dilution) using serial 10-fold dilutions of experimental samples. Primer efficiencies ranged between 95% and 105% and were defined as $(10^{-1/\text{slope}} - 1) \times 100$, using the slope of the calibration curve. qPCR run-specific and primer-specific amplification efficiencies were determined. Normalized relative quantification was performed with Biogazelle qBASE software (version 2.4). Optimal reference genes were determined with the GeNORM algorithm. Quantification was based upon qBASE default calculation parameters.

Western blotting. Protein extracts were prepared from at least three adult Pcbp1 mutant mice or Pcbp2 12.5-dpc embryos for each genotype, euthanized as described above. Tissues (colon, spleen, liver, small intestine, or decapitated embryo) were immediately harvested into lysis buffer (1× PBS, pH 7.2, 0.1% SDS, 0.5% Igepal CA-630, protease inhibitor cocktail [11836170001; Roche]) with prechilled instruments and tubes. Homogenized lysates were snap-frozen, thawed on ice, and cleared by centrifugation at 13,000 rpm for 10 min at 4°C. Supernatants were quantified by a Bio-Rad detergent-compatible (DC) protein assay (500-0111; Bio-Rad). Extracts were separated using standard electrophoresis, and proteins were transferred to nitrocellulose. Blocked membranes were probed overnight with primary antibodies (Table 1) at 4°C, washed, and visualized with fluorophore-conjugated secondary antibodies at 1:15,000 in PBS–0.1% Tween–0.1% SDS (IRDye 800CW–anti-rabbit antibody [925-32213] and IRDye 680RD–anti-mouse antibody [925-68072]; Li-Cor, Lincoln, NE). Signal density was measured on a Li-Cor Odyssey CLx imaging platform. Relative expression of Pcbp1 and Pcbp2 signals was determined by normalization to signal density of the housekeeping glyceraldehyde-3-phosphate dehydrogenase (Gapdh) gene using Image Studio, version 3.1. Statistical analysis was performed using GraphPad Prism, version 6.0.

Metabolic profiling. Serum acylcarnitine, amino acid composition, and urine organic acid profiles were determined from five adult mice for each genotype ($Pcbp1^{+/+}$, $Pcbp1^{+/em2}$, $Pcbp2^{+/+}$, and $Pcbp2^{+/-}$) by mass spectrometry in the metabolism core facility at the Children's Hospital of Philadelphia. Measurements were compared to established reference values for adult mice as determined by the core facility. No values fell outside the normal range for all genotypes tested.

Transcriptome sequencing (mRNA-Seq). Fetal liver was dissected from Pcbp2 wild-type and homozygous null embryos at 12.5 dpc. Embryo viability was verified by direct visualization of a heartbeat and blood circulation. Tissue was placed into TRIzol reagent (catalog number 15596-018; Life Technologies) and disrupted by pipetting, and total RNA was purified according to the manufacturer's protocol, with modifications. Aqueous-phase separation was performed at 16,000 × *g* for 15 min at 4°C

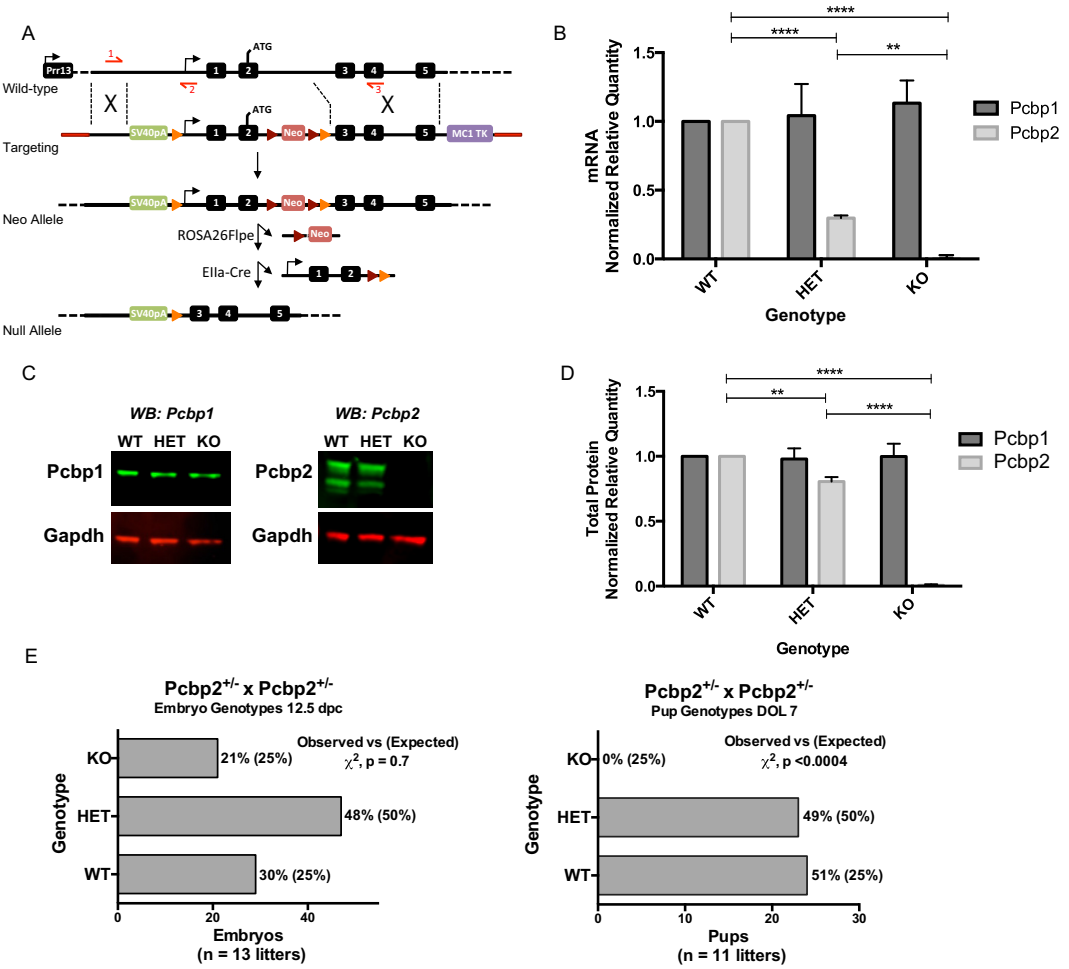

FIG 1 Homozygous inactivation of the *Pcbp2* results in embryonic lethality. (A) Generation of an inactivated Pcbp2 locus by deletion of the promoter and first two exons. The top diagram (wild-type) displays a schematic of the murine Pcbp2 locus on chromosome 15 along with the 5′ adjacent Prr13 gene. Promoters (bent arrows) and the Pcbp2 translational start site (ATG) are noted. The targeting vector for homologous recombination is shown below. An SV40 polyadenylation sequence (SV40pA) was inserted 5′ to the Pcbp2 promoter, and a neomycin selection cassette flanked by Flp recognition target (FRT) sites (red triangles) was introduced into intron 2. The recombined mutant allele (Neo allele), shown on the third line, was subsequently modified by crosses with mice expressing Cre recombinase (EIIa-Cre). Primer sites used for multiplex PCR genotyping are depicted (red arrows) in the wild-type locus diagram. Neo, neomycin selection cassette; MC1 TK, thymidine kinase negative selection cassette. (B) Targeted deletion of the Pcbp2 promoter and 5′ exons eliminates mRNA expression. Total RNAs from Pcbp2 wild-type (WT), heterozygous (HET), and null (knockout, KO) 12.5-dpc embryos were analyzed by reverse transcription-qPCR for Pcbp1 and Pcbp2 mRNA expression. The data are represented relative to the geometric mean of the expression of three independent internal controls: Gapdh, PP1A, and Rpl29 mRNAs. The levels of the normalized expression of Pcbp2 and Pcbp1 mRNAs from the wild-type loci were defined as 1.0. The standard error for each sample is shown (minimum of three biological replicates per genotype). Statistical significance was determined by two-way analysis of variance and Tukey's multiple-comparison test. (C) Pcbp2 protein expression is lost in Pcbp2$^{-/-}$ mice without compensatory changes in Pcbp1 protein levels. Representative Western blot from wild-type, heterozygous, and knockout embryos. (D) Pcbp2 protein expression is lost in Pcbp2$^{-/-}$ mice. Protein signal density from the experiment shown in panel C was quantified from a minimum of six biological replicates per genotype. Protein expression was normalized to Gapdh expression (means ± SE). Statistical significance was determined by a two-tailed *t* test. (E) Pcbp2$^{-/-}$ progeny are lost between 12.5 dpc and day of life 7. The observed percentages of 12.5-dpc embryos (left graph) and live pups 1 week postpartum (right graph) are shown. The expected percentage based upon standard Mendelian inheritance is noted (observed and expected, as indicated). A significant difference between the expected versus observed Pcbp2$^{-/-}$ genotype was demonstrated by the chi-square statistical test [χ^2 (2, n = 47) = 16.01, $P < 0.0004$]. There was no significant difference between expected versus observed genotypes in embryos at 12.5 dpc [χ^2 (2, n = 97) = 0.71, P = 0.70]. DOL, day of life; dpc, days postcoitum. **, $P < 0.01$; ****, $P < 0.0001$.

using phase lock gels (2302830; 5 Prime) to minimize organic solvent carryover.

mRNA sequencing libraries were then generated from 300 nanograms of total RNA using a TruSeq stranded mRNA library prep kit (RS-122-2101; Illumina). Reads were trimmed with Cutadapt and mapped with TopHat2, and gene expression was quantified using HTSeq (54–56). DESeq2 was used to perform differential expression analysis (57).

Nucleotide sequence accession number. All sequencing data generated in this study have been deposited in the Gene Expression Omnibus (GEO) database under accession number GSE72491 (available at http://www.ncbi.nlm.nih.gov/geo/).

RESULTS

Generation of a Pcbp2-null allele. The Pcbp2 locus was modified in V6.5 embryonic stem cells by flanking the Pcbp2 promoter and first two exons with *loxP* recombination sequences using standard recombineering and homologous recombination approaches

(Fig. 1). An SV40pA transcriptional termination sequence was simultaneously inserted upstream of the 5′ *loxP* site to eliminate potential transcriptional read-through from an adjacent, active gene locus (*Prr13*). Prr13 mRNA expression was specifically assayed and found to be unaltered in adult $Pcbp2^{flox/flox}$ and $Pcbp2^{-/-}$ mice compared to that in wild-type littermates, arguing against local off-target effects of the Pcbp2 mutant allele (data not shown). Furthermore, mice carrying the Pcbp2 mutant allele (both homo- and heterozygous floxed) were normal phenotypically and demonstrated normal reproduction (data not shown). Mice carrying the Pcbp2 floxed locus ($Pcbp2^{+/flox}$) were crossed with C57BL/6 EIIa-Cre lines to generate a Pcbp2-null allele ($Pcbp2^{+/-}$) (Fig. 1A). Loss of expression from this null allele in embryos was confirmed by Western blotting and quantitative PCR (Fig. 1B to D). Of note, Pcbp2 mRNA expression in heterozygotes was decreased ~70% compared to that in wild-type mice, which was below the 50% reduction expected for a single allele mutation (Fig. 1B). In contrast, Pcbp2 protein levels were reduced by 20% relative to the levels in wild-type animals, which was above the 50% expected reduction (Fig. 1D). Importantly, the presence of both mutant alleles results in complete loss of Pcbp2 mRNA and protein expression in embryos. Differences in the relative abundances of Pcbp2 mRNA and protein in heterozygotes relative to the expected values was attributed to binding of Pcbp2 protein to the Pcbp2 mRNA 5′ untranslated region (UTR) (based on Pcbp2 RNA cross-linking and immunoprecipitation followed by high-throughput sequencing [CLIP-seq] studies to be reported separately), as is observed for multiple mRNAs encoding RNA-binding proteins (see also the Discussion) (58, 59).

Generation of a Pcbp1-null allele. One-cell C57BL/6 embryos were microinjected with the set of TALEN mRNAs designed to flank the start codon of the mouse Pcbp1 locus (Fig. 2A) (60, 61). Both right and left TALEN recognition sequences contained at least three mismatches with the corresponding region of the mouse Pcbp2 locus. Injected embryos were reimplanted in pseudopregnant females and brought to term. DNA of live-born progeny was screened for targeted deletions by PCR amplification across the targeted region, followed by Sanger sequencing of the amplified product. Frameshift mutations that resulted in premature translational stop codons were identified in five founder mice from a total of 42 progeny tested (Fig. 2A). Lines were established from two of these founders (em2 and the em6). *In silico* screening for potential off-target sites using a variety of algorithms and parameters (see Materials and Methods for details) (45, 46) failed to reveal any high-likelihood targets. PCR amplification and Sanger sequencing directly ruled out off-target cleavage of the Pcbp2 locus (Fig. 2B).

The loss of Pcbp1 expression from the two Pcbp1 frame-shifted alleles was confirmed by demonstrating a 62 to 64% decrease of Pcbp1 protein levels on Western blots in both $Pcbp1^{+/em2}$ and $Pcbp1^{+/em6}$ mice (Fig. 2D). Of note, levels of the corresponding Pcbp1 mRNAs were equivalent to those of the wild-type littermates (Fig. 2C). The loss of protein expression due to the early nonsense mutation in the $Pcbp1^{+/em2}$ and $Pcbp1^{+/em6}$ mice and preservation of the encoding mRNA levels were fully consistent with immunity of the intronless mRNAs from the nonsense-mediated decay (NMD) pathway (see also the Discussion). These data confirmed that TALEN-mediated gene editing of the Pcbp1 locus resulted in the generation of two null alleles: $Pcbp1^{em2}$ and $Pcbp1^{em6}$. Except where noted, all subsequent experiments were conducted using the $Pcbp1^{em2}$ line.

Haploinsufficiency for *Pcbp1* and *Pcbp2* results in mild weight attenuation. The studies noted above demonstrate viability of adult mice haploinsufficient for Pcbp1 and Pcbp2. The percentage of heterozygous pups at 1 week of life from either $Pcbp1^{+/em2} \times Pcbp1^{+/em2}$ or $Pcbp2^{+/-} \times Pcbp2^{+/-}$ intercrosses trended slightly below that expected, but this difference did not reach significance (Pcbp1, $P = 0.31$; Pcbp2, $P = 0.14$; Fisher's exact test). These findings suggested that Pcbp1 or Pcbp2 haploinsufficiency is consistent with adult life but may result in a marginal survival disadvantage during the first week after birth.

The potential impact of haploinsufficiency on extrauterine growth was assessed by serial weight measures over the first 20 weeks of life. These studies revealed significantly lower weights in $Pcbp2^{+/-}$ mice than in their gender-matched wild-type littermates (male, weeks 1, 2, and 4 to 20, $P < 0.05$; female, weeks 2 through 20, $P < 0.05$) (Fig. 3B). A similar negative impact on the weight curve was observed in the analysis of the Pcbp1-haploinsufficient mice (male, weeks 2 to 20, $P < 0.05$; female, weeks 2 to 20, $P < 0.05$) (Fig. 3A). These lower weights were evident in the Pcbp1- and Pcbp2-haploinsufficient mice prior to weaning and persisted after mice were transitioned to standard mouse chow (21 days of life). Analysis of weights in litters generated from heterozygote × heterozygote intercrosses, as well as wild-type × heterozygote intercrosses, yielded the same mild weight differences (data not shown). Mice heterozygous for the Pcbp1- and Pcbp2-null alleles were otherwise grossly normal. Heterozygous intercrosses (Pcbp1 × Pcbp1 and Pcbp2 × Pcbp2) were successful, and litter sizes were commensurate with selective dropout of null embryos. These observations suggest that fecundity in Pcbp1 and Pcbp2 heterozygotes was not impaired in the heterozygous state.

The cause for the lower weights was investigated by a screen for defects of lipid, organic acid, and amino acid metabolism; the data were equivalent in the comparison of the Pcbp1 or Pcbp2 wild-type versus corresponding heterozygous adult mice (data not shown). The possibility that the postnatal weight differences reflected intrauterine growth retardation was assessed in the Pcbp2-haploinsufficient embryos by measurements of crown-rump length and placental diameter, both of which were identical between $Pcbp2^{+/-}$ embryos and their wild-type littermates (Fig. 3C). (A parallel study of the Pcbp1 could not be done due to the dropout of the embryos at the preimplantation stage [see below].) We next tested whether Pcbp1 and Pcbp2 compound heterozygous mice manifest a more severe weight attenuation phenotype than the simple heterozygotes. From 12 litters (35 pups), the Mendelian expectation was ~9 $Pcbp1^{+/em2}$ $Pcbp2^{+/-}$ animals (25%); we observed four live births (11%) (Fig. 3D). Of these, only one female survived beyond the first week of life and was severely runted (Fig. 3E). While these data suggest a gene dose or dosage imbalance effect in Pcbp compound heterozygous mice (62), the etiology of the low weights in the $Pcbp1^{+/em2}$, $Pcbp2^{+/-}$, and $Pcbp1^{+/em2}$ $Pcbp2^{+/-}$ mice remained undefined.

The Pcbp2 and Pcbp1 loci are individually essential for embryonic viability. Intercrosses of heterozygotes to generate mice that are homozygous for the Pcbp1 or Pcbp2 null alleles failed to generate homozygous null progeny at term (Fig. 1E and 2E). Genotyping of 5- to 7-day-old pups from intercrosses of $Pcbp2^{+/-}$ males and females revealed only wild-type and heterozygous progeny (Fig. 1E, left panel). The absence of mice

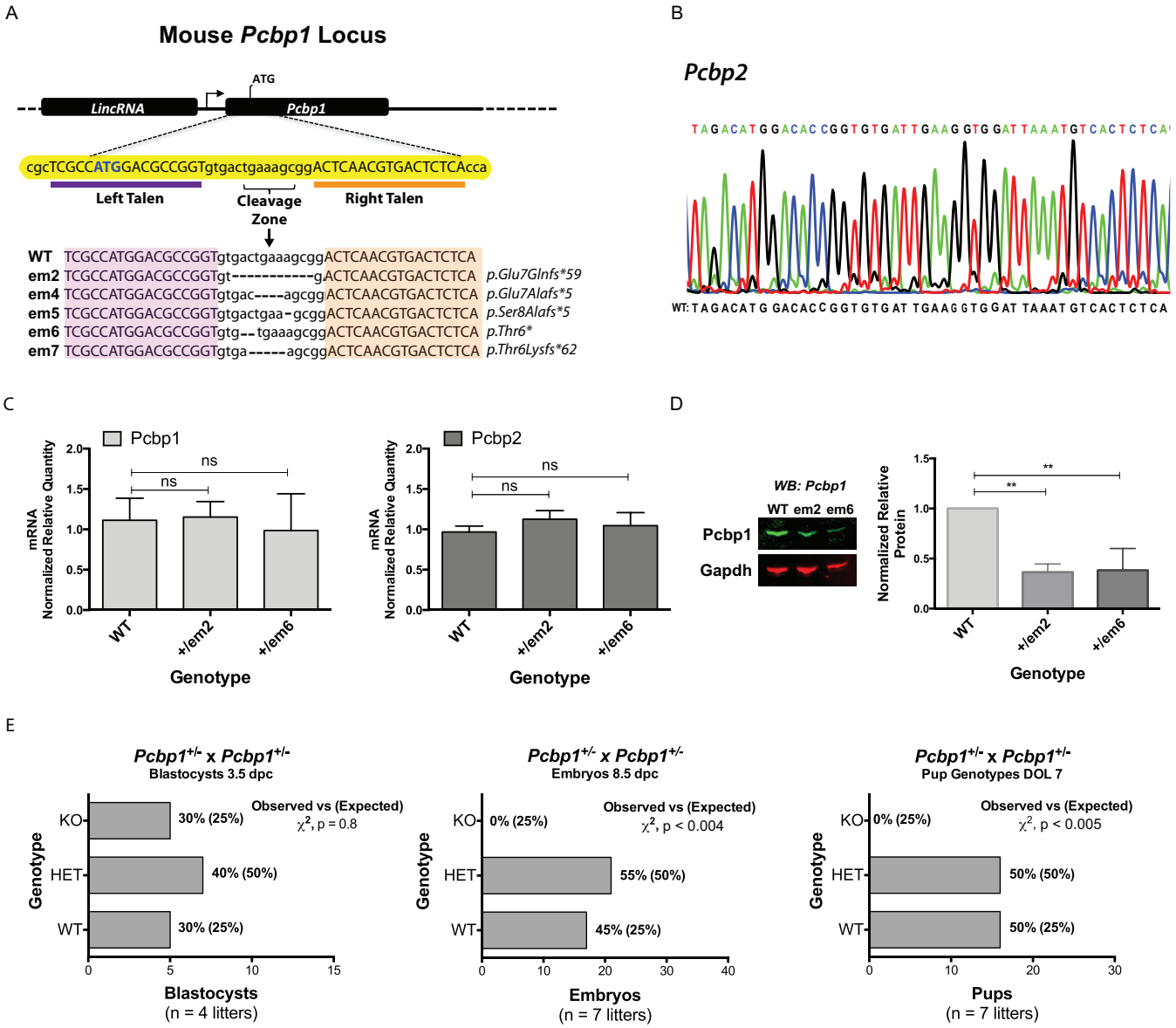

FIG 2 Ablation of protein expression from the Pcbp1 locus by TALEN-mediated deletion. (A) Introduction of deletions 3′ to the translation initiation codon by TALEN-targeted cleavage and nonhomologous end joining. Schematic of the mouse Pcbp1 locus with left (purple) and right (orange) TALEN target sequences indicated. The translation initiation codon is underlined. TALEN-mediated cleavage and nonhomologous end joining generated five null (deletion/frameshift) alleles (em2, -4, -5, -6, and -7). Alignments to the WT sequence are shown; dashes denote deleted bases. A description of the resulting protein variant is shown. (B) Analysis for off-target mutation at the Pcbp2 locus. Sanger sequencing confirms that the region of the Pcbp2 locus corresponding to the Pcbp1-induced mutation is intact. The wild-type sequence is shown for comparison. (C) Wild-type levels of mRNA are generated from the Pcbp1 mutant allele. Total RNAs from adult Pcbp1$^{+/+}$ (WT), Pcbp1$^{+/em2}$ (em2), and Pcbp1$^{+/em6}$ (em6) mice were analyzed by quantitative PCR for Pcbp1 and Pcbp2 expression. Normalization and statistical analysis were done as noted in the legend to Fig. 1B. (D) TALEN-mediated deletion at the Pcbp1 locus eliminates protein expression. A representative Western blot from wild-type and heterozygous (Pcbp1$^{+/em2}$ and Pcbp1$^{+/em6}$) mice is shown. Protein signal density was quantified from a minimum of six biological replicates per genotype. The mean and standard error of Pcbp1 protein expression normalized to Gapdh expression is shown. Statistical significance was determined by a two-tailed *t* test. (E) Homozygosity for the em2 allele (Pcbp1$^{em2/em2}$) is embryonic lethal. The percentages of observed genotypes in 3.5-dpc blastocysts, 8.5-dpc embryos, and pups 1 week postpartum are shown. The expected percentage based upon standard Mendelian inheritance is noted (observed and expected, as indicated). A significant difference between the expected versus observed Pcbp1$^{em2/em2}$ genotypes in 8.5-dpc embryos and pups was demonstrated by a chi-square statistical test [χ^2 (2, n = 38) = 11.55, $P < 0.004$, and χ^2 (2, n = 32) = 10.67, $P < 0.005$, respectively]. There was no significant difference between expected versus observed genotypes in blastocysts at 3.5 dpc [χ^2 (2, n = 17) = 0.47, $P = 0.79$]. DOL, day of life; dpc, days postcoitum; ns, not significant; **, $P < 0.01$.

homozygous for the Pcbp2-null allele was highly significant (chi-square, $P < 0.04$). These data demonstrated that haploinsufficiency for Pcbp2 is compatible with adult life and that embryos entirely lacking Pcbp2 do not survive to term gestation (Fig. 1E, right panel). Pcbp1$^{em2/em2}$ blastocysts harvested at 3.5 days postcoitus (dpc) had the expected Mendelian ratios (Fig. 2E, left panel) but homozygous null embryos were not detectable at 8.5 dpc (Fig. 2E, middle panel) or in adults (Fig. 2E, right panel). In

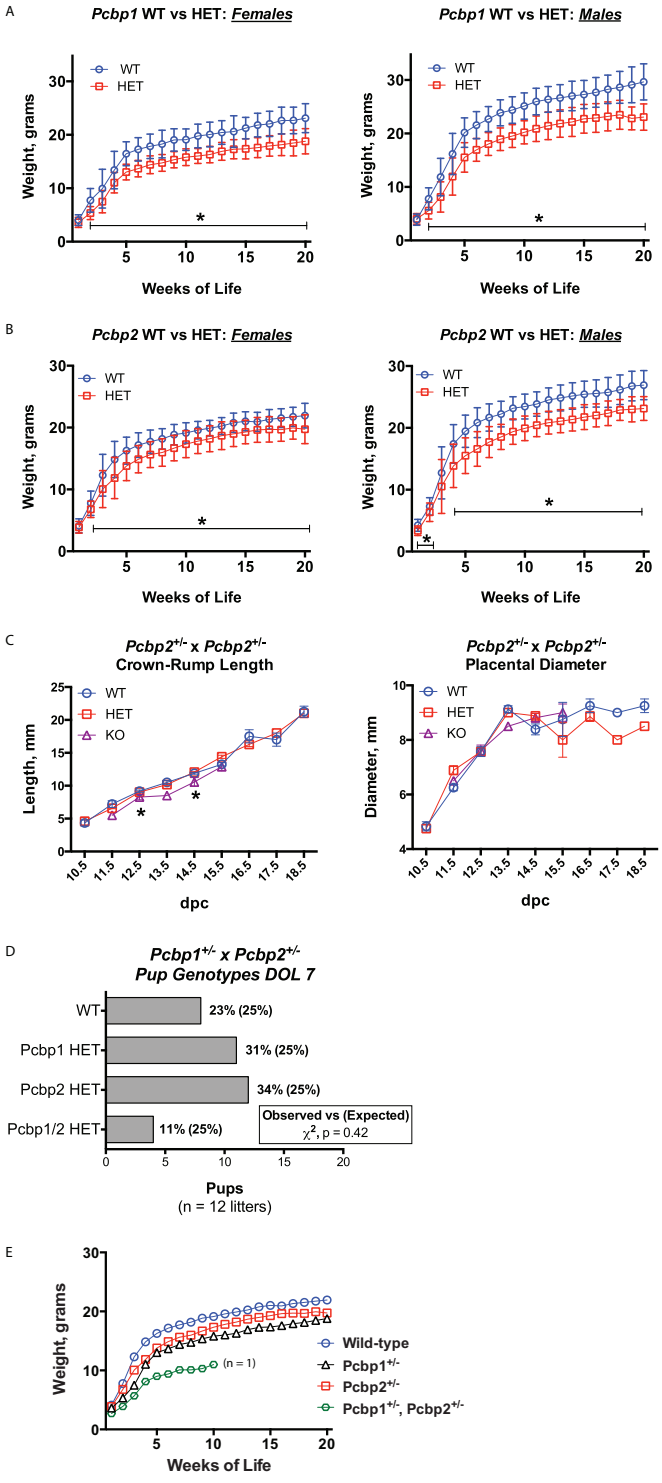

FIG 3 Mice heterozygous for the *Pcbp1* and *Pcbp2* null mutations have reduced weight compared to weights of normal littermates. (A) Subnormal weight gain in Pcbp1$^{+/em2}$ mice. A time course (week 1 through week 20) of weight measures comparing Pcbp1 wild-type to haploinsufficient mice for both genders is shown. *, $P < 0.02$, by unpaired *t* test for each time point. Note that there is no significant difference in the weights of the pups at 1 week. (B) Subnormal weight gain in Pcbp2$^{-/+}$ mice. Mice were analyzed as described in the legend of panel A. Note that there is no significant difference in the weights of the pups at 1 week. (C) Mid-to-late gestation crown-rump measures and placental diameters are normal for Pcbp2 (HET) and homozygous null (KO) mice. *, $P < 0.04$, by unpaired *t* test; dpc, days postcoitum. (D) Pcbp1 and Pcbp2 compound heterozygous mice are viable at birth. The observed percentages of live pups 1 week postpartum are shown. There was no significant difference between expected versus observed genotypes by a chi-square statistical test [χ^2 (3, $n = 35$) = 2.60, $P = 0.42$]. (E) Severely runted phenotype in Pcbp1$^{+/em2}$ Pcbp2$^{+/-}$ compound heterozygous mouse. A time course of weight measures for female mice of each genotype is shown. Average weights of wild-type and Pcbp heterozygous mice are plotted for reference.

contrast, Pcbp2$^{-/-}$ embryos were viable (positive heart beat and normal body structure) at 12.5 days but did not survive beyond 14.5 to 15.5 dpc (data not shown). Gross evaluation of Pcbp2$^{-/-}$ embryos was notable for large focal areas of hemorrhage and subcutaneous edema in most specimens at 13.5 dpc and for microhemorrhage in a minority at 12.5 dpc (Fig. 4 and data not shown). The distinct timing and manifestations of embryonic lethality for Pcbp1$^{-/-}$ and Pcbp2$^{-/-}$ embryos lead us to conclude that the two genes play distinct and essential roles in embryonic development.

Hematopoietic defects in Pcbp2-null embryos. The hemorrhage and subcutaneous edema phenotypes in the Pcbp2$^{-/-}$ embryos led us to consider underlying abnormalities in the hematopoietic, cardiac, and vascular systems. Global edema and pericardial effusion in isolation can be direct manifestations of embryonic heart failure, and when associated with widespread hemorrhage, these findings may also reflect primary vascular abnormalities. While light-microscopic analysis of the cardiac and vascular systems failed to reveal defects in the midgestational Pcbp2-null mice, ongoing detailed studies (outside the scope of this report) are in progress to further explore these issues.

We next explored potential hematopoietic defects in Pcbp2-null embryos. Pcbp2 has been mechanistically linked to both nuclear and cytoplasmic posttranscriptional controls over globin gene expression (20, 36, 63). The *in vivo* role of Pcbp2 in hematopoiesis was facilitated by the fact that Pcbp2-null embryos remain uniformly viable at 12.5 dpc, a developmental time point where hematopoiesis is well established in the fetal liver. Similar studies were not possible in Pcbp1-null embryos due to preimplantation lethality that occurs well in advance of hematopoietic differentiation. Erythroid maturation profiles were established in Pcbp2 wild-type, heterozygote, and null erythroblasts in 12.5-dpc liver, the site of robust expansion of the definitive erythroid lineage (64). Cells were analyzed by fluorescence-activated cell sorting (FACS) using a combination of two extensively validated markers of erythroid development, CD71 and Ter119. The presence and levels of these two cell surface proteins can be used to follow maturation of the hematopoietic progenitor (stage S0) to mature erythroblasts (stage S4/5) (51). This analysis revealed a significant increase in the representation of immature (S1) cells and a reciprocal decrease in the populations of more mature (S3 and S4/5) erythroblasts in Pcbp2$^{-/-}$ embryos compared to levels of heterozygote and wild-type littermates (Fig. 5A and B). There were no appreciable differences in the percentages of necrotic cells in mutant and wild-type embryos at the time of analysis (data not shown). Evaluation of complete blood counts in the adult Pcbp2 heterozygotes failed to reveal any abnormalities in red cell number or cellular parameters (data not shown). These data define a significant impairment in the pathway of erythroid maturation in Pcbp2$^{-/-}$ embryos.

As megakaryocytes and erythroblasts are derived from a common megakaryocyte-erythroid progenitor (MEP), the combined

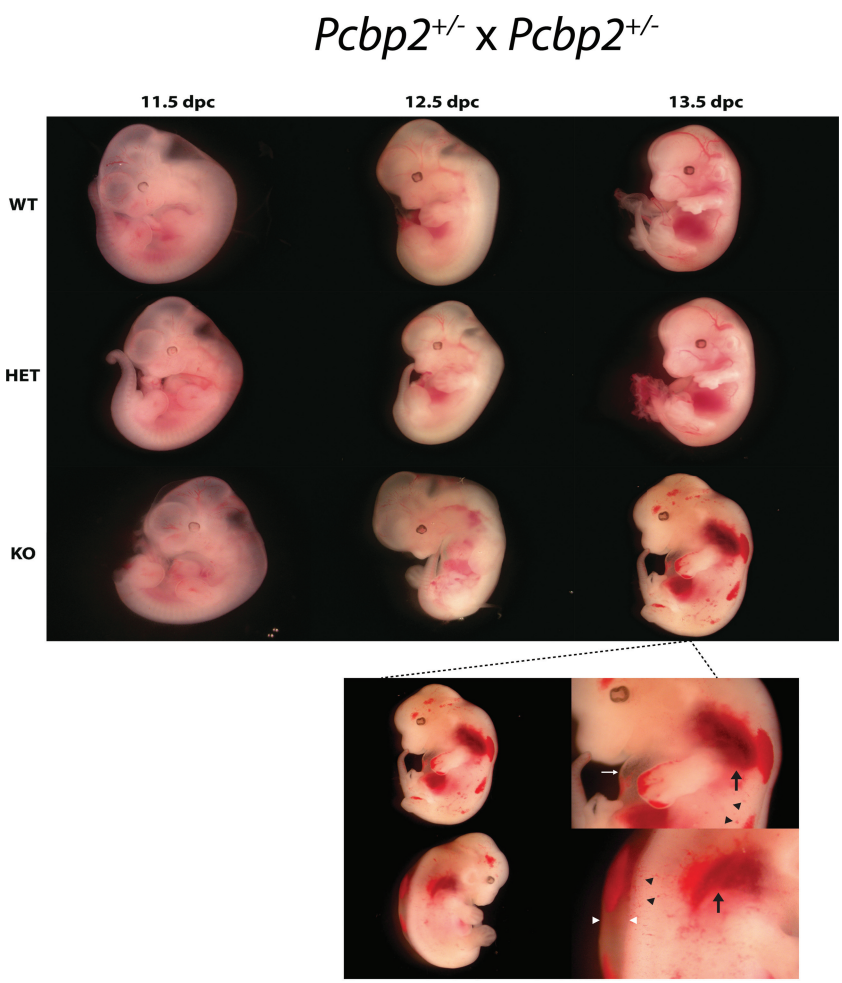

FIG 4 Midgestational lethality of Pcbp2$^{-/-}$ embryos is associated with gross hemorrhage and edema. Littermate embryos from Pcbp2$^{+/-}$ × Pcbp2$^{+/-}$ crosses were analyzed at three midgestational time points (11.5 dpc, 12.5 dpc, and 13.5 dpc). Genotypes are indicated to the left of the respective embryos. Images are magnified for optimal viewing and are not to scale. Two views of the 13.5-dpc Pcbp2$^{-/-}$ embryo are depicted (dashed lines). Adjacent magnified views portray pericardial effusion (white arrow), subcutaneous edema (white arrowheads), and macro- and microhemorrhages (black arrows and black arrowheads, respectively).

defect in erythroid maturation and presence of subcutaneous hemorrhages seen in Pcbp2$^{-/-}$ embryos led us to hypothesize a defect in megakaryopoiesis in null embryos (65, 66). To evaluate megakaryopoiesis, 12.5-dpc liver tissues from Pcbp2 wild-type and mutant embryos were stained for a megakaryocyte marker (von Willebrand factor [vWF]). Quantification of vWF-positive cells morphologically verified as megakaryocytes revealed a stepwise reduction in embryonic megakaryocytes quantified in Pcbp2 wild-type, heterozygous, and Pcbp2-null embryos (mean, 28.3, 22.2, and 7.0 vWF-positive cells per high-power field [40×], respectively) with the decrease in the null embryos being highly significant compared to that of the two other groups (Fig. 6A and B). Similar findings were identified in cells analyzed by FACS using the megakaryocyte marker CD41 (Fig. 6C). Evaluation of complete blood counts in the adult Pcbp2 heterozygotes revealed a downward trend in mean platelet counts between Pcbp2$^{+/+}$ and Pcbp2$^{+/-}$ mice (wild-type, 1,400 × 10^3/μl ± 83 × 10^3/μl, versus heterozygous, 1,165 × 10^3/μl ± 99 × 10^3/μl; values are means ± standard errors [SE]) (data not shown). No differences were identified in complete blood counts between Pcbp1$^{+/+}$ and Pcbp1$^{+/-}$ mice (data not shown). We conclude from these data that embryonic megakaryopoiesis is defective in Pcbp2$^{-/-}$ embryos and speculate that this phenotype may reflect impairment of the common megakaryocyte-erythroid progenitor or upstream progenitors.

Transcriptome analysis of embryonic liver supports a significant impact of Pcbp2 ablation on the development of the hematopoietic and megakaryocyte lineages. To investigate changes in hematopoietic gene expression impacted by the loss of Pcbp2, we performed mRNA-seq on wild-type and Pcbp2$^{-/-}$ 12.5-dpc fetal liver tissue. Definitive erythropoiesis first arises in the mouse fetal liver at 9.5 dpc while multilineage (myeloid, lymphoid, erythroid, and megakaryocytic) hematopoiesis is well established at this site by 12.5 dpc (64). We identified a total of 515 genes that were differentially expressed in Pcbp2$^{-/-}$ fetal liver compared to expression levels in the wild-type (Wald test, adjusted *P* value of <0.001) (Fig. 7A). Of these, 172 genes displayed at least a 2-fold decrease, and 41 genes had a 2-fold increase in Pcbp2$^{-/-}$ fetal liver mRNA ($\log_2$ fold change ≥ 1) (see Table S1 in the supplemental material). The transcriptome comparisons confirmed the ex-

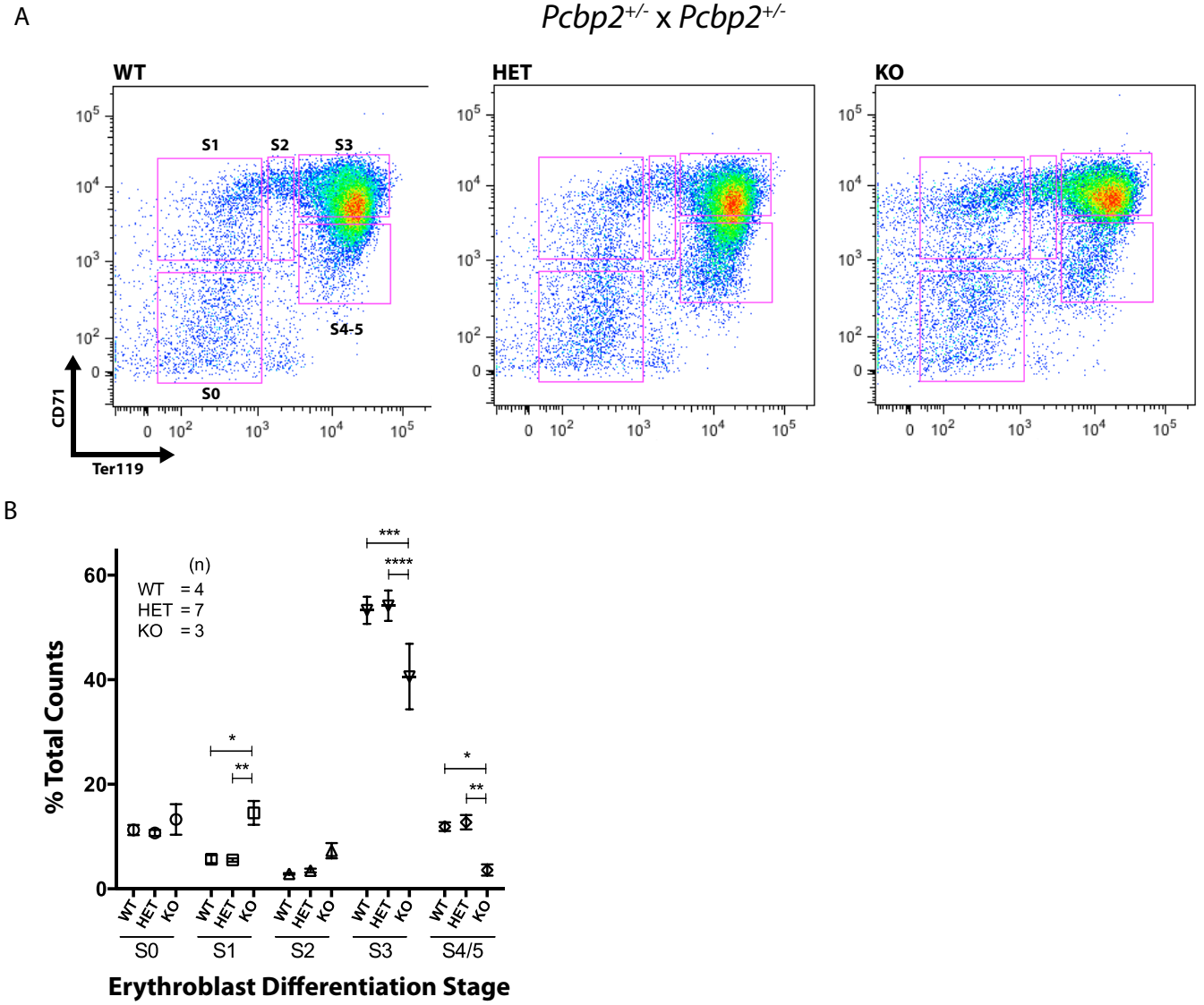

FIG 5 Erythroid differentiation is impaired in 12.5-dpc *Pcbp2*$^{-/-}$ embryos. (A) Flow cytometry assay of embryonic day 12.5 fetal liver cells from Pcbp2 wild-type (WT), heterozygous (HET), and null (KO) embryos. FACS analyses of cells stained with CD71 and Ter119 are depicted. The images are representative of at least three biological replicates. Profiles are divided into five subsets (S0 to S4/5) corresponding to stages of erythroblast differentiation (S0, early; S4/5, late) (51). (B) Quantitative analysis of S0 to S4/5 subsets from the experiment shown in panel A. Data points represent the means and SE of total cell counts from each erythroid subset stratified by genotype. Statistical significance was determined by two-way analysis of variance and a multiple-comparison test (*, $P < 0.05$; **, $P < 0.01$; ***, $P < 0.001$; ****, $P < 0.0001$). The number (n) of independent assays for each respective genotype is noted in the inset.

pected loss of Pcbp2 along with a dramatic repression in the levels of two major erythroid mRNAs, encoding α- and β-globin (Fig. 7A). Pcbp1 mRNA expression was unchanged in Pcbp2$^{-/-}$ fetal liver compared to the level in controls (Fig. 7A). The impact of Pcbp2 ablation on a subset of transcripts critical to erythroid, megakaryocyte, and myeloid differentiation and function was selected for validation by qPCR (Fig. 7B and C). The strong correlation between gene expression measures across techniques (Spearman coefficient; $R = 0.95$) (Fig. 7B) confirmed the repression of mRNAs critical to hemoglobin biogenesis and erythroid differentiation (Fig. 7C). This finding was reinforced by a gene ontology (GO) analysis (DAVID) (Fig. 7D; see also Table S2 in the supplemental material) (67). Furthermore, there was a significant decrease in transcripts essential for megakaryocyte development and function (*Ppbp*, *Pf4*, *Gp1bb*, and *Vwf*) in the Pcbp2$^{-/-}$ fetal liver relative to that of wild-type embryos (Fig. 7C; see also Table S1). These data reveal marked alterations in the 12.5-dpc Pcbp2$^{-/-}$ fetal liver transcriptome, consistent with an impairment in erythroid and megakaryocyte differentiation.

Gene transcriptional profiles that characterize specific hematopoietic lineages, including differentiated erythroid cells, have been well characterized in both human and mouse hematopoiesis (68, 69). To determine if the observed changes in the Pcbp2$^{-/-}$ fetal liver transcriptome reflected a global impact on hematopoiesis or were limited to expression differences within a specific hematopoietic lineage(s), we compared the expression of signature genes in five major lineages (hematopoietic stem cells, differentiated erythroid cells, granulocyte/monocytes, T cells, and B

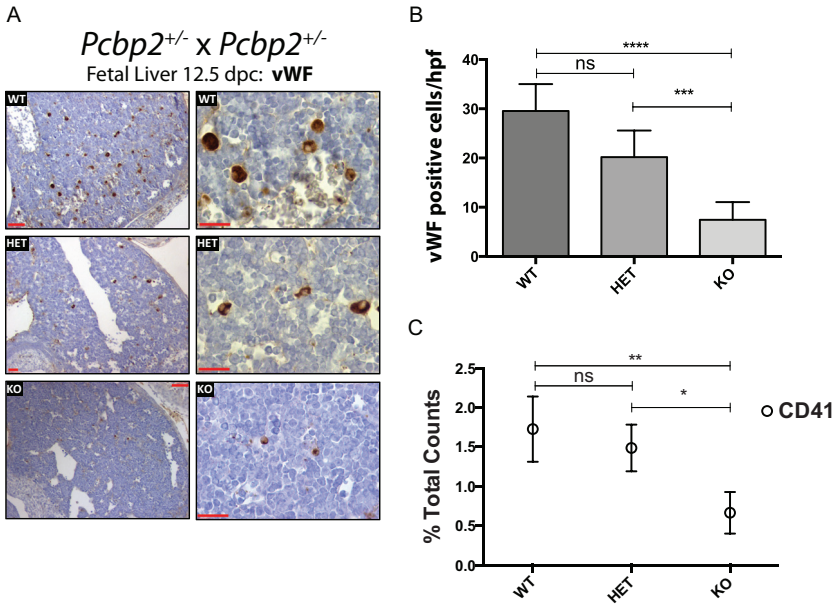

FIG 6 Depletion of the megakaryocyte population in *Pcbp2*$^{-/-}$ fetal liver. (A) Fixed sagittal sections from Pcbp2 12.5-dpc embryos stained with von Willebrand factor (vWF) to identify megakaryocytes in the fetal liver. The genotypes of the littermate embryos are indicated in each respective frame. (B) Quantification of vWF-positive cells per high-power field (hpf) for each genotype. Data represent means with standard deviations from at least four biological replicates per genotype. Statistical significance was determined by one-way analysis of variance and Tukey's multiple-comparison test (ns, not significant; ***, $P < 0.001$; ****, $P < 0.0001$). (C) Quantitative analysis of Pcbp2 wild-type (WT), heterozygote (HET), and null (KO) 12.5-dpc fetal liver cells evaluated by flow cytometry for megakaryocyte (CD41) lineage markers. Data points represent the means and SE of total cell counts stratified by genotype. Statistical analysis was performed as noted in the description of panel B. *, $P < 0.05$; **, $P < 0.01$.

cells) (68) in wild-type and knockout tissue. This analysis revealed that genes characterizing differentiated erythroid cells and granulocytes/monocytes were significantly downregulated (Mann-Whitney test, $P < 2.2 \times 10^{-16}$ and $P < 2.5 \times 10^{-16}$, respectively) (Fig. 7E). In stark contrast, genes characterizing hematopoietic stem cell, B cell, and T cell lineages were unaffected or upregulated (Mann-Whitney test, $P < 2.4 \times 10^{-2}$, $P < 0.02$, and $P < 4.1 \times 10^{-4}$, respectively) (Fig. 7E). Interestingly, when we assessed fetal liver mature phagocyte cell numbers by FACS, we did not observe an alteration in these cell types in Pcbp2-null tissue (data not shown). When coupled to the transcriptional profiles, these data point to an impact of Pcbp2 ablation on early myeloid progenitors with recovery in neutrophil and monocyte terminal differentiation.

We utilized previously defined gene signatures that distinguish between erythroid and megakaryocyte lineages from murine fetal liver primary cells (14.5 dpc) (69) to determine if Pcbp2 had a specific impact upon erythroid versus megakaryocyte gene expression. We found that erythroid and megakaryocyte lineage genes were both downregulated in Pcbp2$^{-/-}$ fetal livers (Mann-Whitney test, $P < 2.2 \times 10^{-16}$ and $P < 2.6 \times 10^{-4}$, respectively) (Fig. 7F). These observations are fully consistent with our direct studies of erythroid and megakaryocyte lineages (Fig. 5 and 6) and lead us to conclude that absence of Pcbp2 results in a marked downregulation of gene expression programs important for the megakaryocyte-erythrocyte progenitor (MEP) and descendant lineages

DISCUSSION

Here, we present evidence that the Pcbp1 and Pcbp2 loci are individually essential for mouse embryonic viability and impact distinct pathways critical to embryonic development. Embryos lacking Pcbp1 lose viability at 4.5 to 8.5 dpc while the Pcbp2-null embryos develop normally through 12.5 to 13.5 dpc. The nonredundant contributions of the two paralogous proteins could reflect distinct biochemical properties, distinct tissue specificities, and/or differences in developmentally timed expression patterns. Pcbp1 and Pcbp2 have widespread and overlapping tissue distribution and are expressed at robust levels in both embryonic and adult mammalian tissues ((16, 27, 44). A number of *ex vivo* models support distinct biochemical functions for Pcbp1 and Pcbp2. For example, Pcbp1 is uniquely capable of regulating epithelial-mesenchymal transitions and stabilizing vascular nitric oxide synthase transcripts (37, 42, 70), while Pcbp2 specifically controls tumor suppressor genes in chronic myelogenous leukemia, poliovirus translation, and HIV gene expression (39–41). Thus, our *in vivo* analysis of embryogenesis is concordant with previous *ex vivo* studies in demonstrating that Pcbp1 and Pcbp2 play distinct roles in organism function.

The retrotransposition event that generated the Pcbp1 locus from a processed Pcbp2 transcript (16) predates the mammalian radiation (~80 million years ago) and is estimated to have occurred ~400 to 500 million years ago (15, 16). The template for the Pcbp1 retrotransposed locus was a minor, alternatively spliced Pcbp2 mRNA that retains an exon that is excluded in >70% of Pcbp2 mRNAs. This exon (exon 8; GenBank accession number NM_005016) encodes a 29-amino-acid auxiliary domain located between the RNA-binding KH domains II and III. Thus, the generation of the Pcbp1 gene captured a minor Pcbp2 isoform via retrotransposition. This evolutionary event served to fix the high-level expression of a Pcbp protein containing this auxiliary domain (16, 71). The stringent conservation of the Pcbp1 open read-

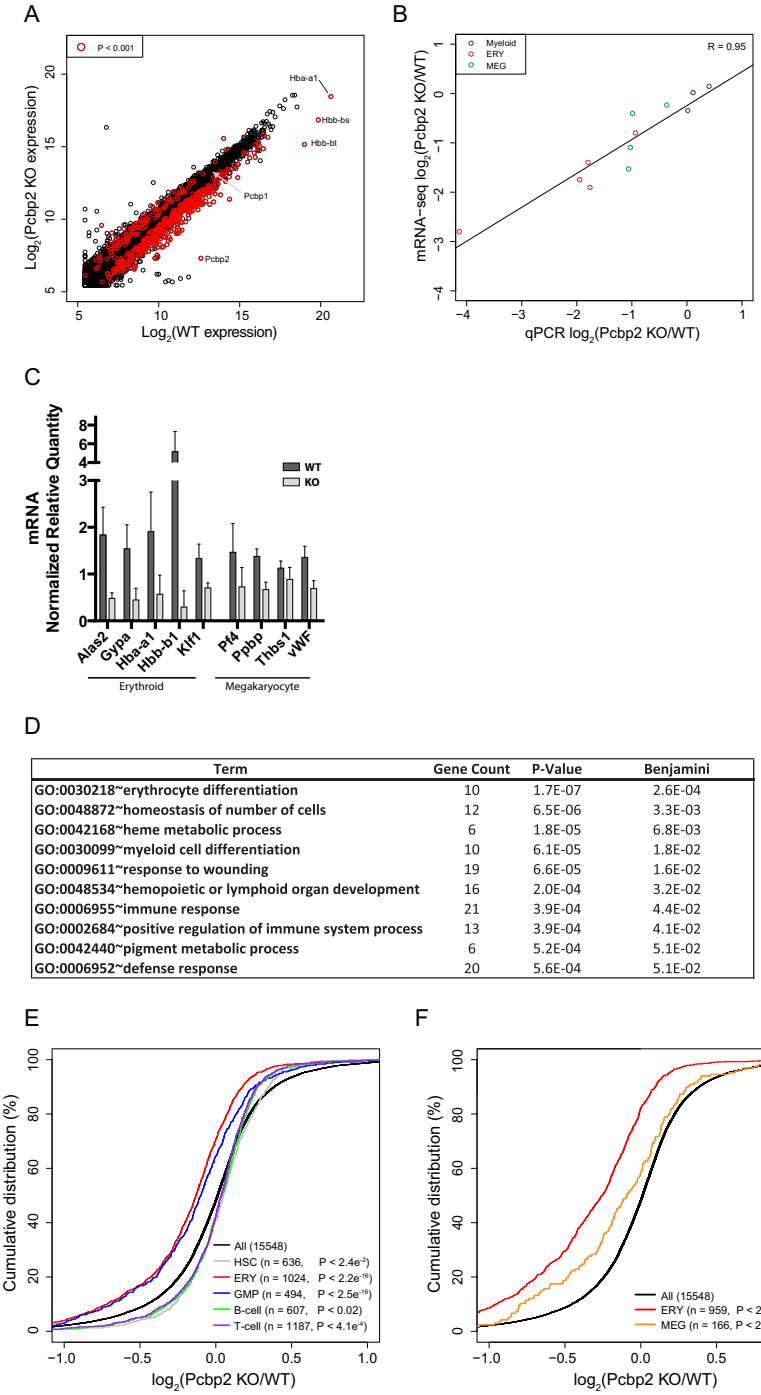

Term	Gene Count	P-Value	Benjamini
GO:0030218~erythrocyte differentiation	10	1.7E-07	2.6E-04
GO:0048872~homeostasis of number of cells	12	6.5E-06	3.3E-03
GO:0042168~heme metabolic process	6	1.8E-05	6.8E-03
GO:0030099~myeloid cell differentiation	10	6.1E-05	1.8E-02
GO:0009611~response to wounding	19	6.6E-05	1.6E-02
GO:0048534~hemopoietic or lymphoid organ development	16	2.0E-04	3.2E-02
GO:0006955~immune response	21	3.9E-04	4.4E-02
GO:0002684~positive regulation of immune system process	13	3.9E-04	4.1E-02
GO:0042440~pigment metabolic process	6	5.2E-04	5.1E-02
GO:0006952~defense response	20	5.6E-04	5.1E-02

FIG 7 Transcriptome analysis of *Pcbp2*$^{-/-}$ fetal liver reveals downregulation of hematopoietic lineage transcriptional programs. (A) Scatter plot of gene expression counts comparing the transcriptomes of wild-type and Pcbp2$^{-/-}$ 12.5-dpc fetal liver. Red circles denote genes that have differential expression reaching statistical significance (Wald test; adjusted *P* value of <0.001). Pcbp1, Pcbp2, and hemoglobin genes are highlighted. Gene expression counts were derived from a variance stabilizing transformation (57). (B) Scatter plot of gene expression changes in *Pcbp2*$^{-/-}$ tissue compared to that in wild-type tissue between mRNA-seq and qPCR data sets. The data analyzed are for selected myeloid (blue; *Cebpa*, *Csf2ra*, and *Mpo*), erythroid (red; *Alas2*, *Gypa*, *Hba-a1*, *Hbb-bs*, and *Klf1*), and megakaryocyte (green; *Pf4*, *Ppbp*, *Thbs1*, and *Vwf*) genes (Spearman coefficient; $R = 0.95$, $P < 2.2 \times 10^{-16}$). (C) Critical megakaryocyte and erythroid lineage genes are decreased in Pcbp2$^{-/-}$ fetal liver. Relative mRNA levels were quantified in Pcbp2 wild-type (WT) and knockout (KO) 12.5-dpc fetal liver by quantitative PCR. (D) DAVID gene ontology (GO) biofunction analysis reveals that Pcbp2-downregulated genes are enriched for erythroid hematopoiesis and heme biosynthetic pathways. (E) Erythroid and granulocyte/monocyte signature genes are downregulated in Pcbp2$^{-/-}$ fetal liver. A cumulative distribution plot of gene expression changes ($\log_2$ fold change) for genes that characterize five distinct human hematopoietic lineages defined by Novershtern et al. (*n* = total number of genes that define each lineage) (68) is shown. All noted *P* values were determined using a Mann-Whitney test. HSC, hematopoietic stem cells; ERY, differentiated erythroid cells; GMP, granulocyte/monocyte progenitor. (F) Murine erythroid and megakaryocyte transcriptional signatures are selectively downregulated in Pcbp2$^{-/-}$ 12.5-dpc fetal liver. A cumulative distribution plot is shown, and statistics are as described for panel E. Mouse erythroid (ERY) and megakaryocyte (MEG) lineage-defining genes (*n*) are as determined by Pimkin et al. (69).

ing frame subsequent to the retrotransposition event suggests that this processed gene has taken on an essential role critical to the cell that is distinct from that of its Pcbp2 progenitor. Our observation that Pcbp1 is required earlier in development than its originating gene supports this hypothesis.

Prior studies have revealed that KH domain mutations that eliminate RNA-binding capacity result in complete loss of protein function (72, 73). Indeed, single point mutations in KH domains that impact RNA binding have been linked to severe human pathology (74). This no doubt contributes to the constraint on sequence divergence in the three KH domains in the Pcbp isoforms. In contrast, selective drift in the auxiliary domain between KH domains II and III (Pcbp1 has 69% amino acid identity to Pcbp2) could permit the evolution of protein structures that can modify RNA-binding affinity and/or facilitate alternative recruitment of RNA processing factors/complexes to target mRNAs. Thus, the capture of this auxiliary region in the retrotransposed Pcbp1 gene would allow substantial functional adaptation distinct from the originating Pcbp2 locus that could comprise a distinct set of posttranscriptional controls essential for organism development.

The Pcbp1-null alleles were generated by TALEN-mediated endonuclease cleavage and subsequent nonhomologous end joining (Fig. 2) (60). Off-target analysis demonstrated that the Pcbp2 locus was intact in the derived Pcbp1 mutant mouse lines, the Pcbp1$^{+/em2}$ and Pcbp1$^{+/em6}$ lines (Fig. 2B and data not shown), and the concordance of embryonic lethality between these two independent founder lines argues against off-target effects contributing to the observed phenotypes. Pcbp1 proteins encoded by the Pcbp1$^{+/em2}$ allele (*p.Glu7Alafs*5*) or Pcbp1$^{+/em6}$ allele (*p.Thr6**) would be severely truncated and most likely unstable, resulting in the 60% decrease in Pcbp1 protein expression in the mice heterozygous for these mutant alleles. The preservation of the encoding Pcbp1$^{+/em2}$ and Pcbp1$^{+/em6}$ mRNAs at wild-type levels is fully consistent with resistance of an intronless Pcbp1 gene transcript to NMD (75, 76).

Pcbp2 protein expression data (Fig. 1C and D) demonstrated that Pcbp2 protein and mRNA expression are reduced by 20% and 70%, respectively, in Pcbp2$^{+/-}$ mice. We postulate that the differences in protein (down 20%) versus mRNA (down 70%) abundance in Pcbp2 heterozygous mice reflect a posttranscriptional autoregulatory circuit. This model is supported by Pcbp2 cross-linked immunoprecipitation and high-throughput sequencing (CLIP-seq) experiments (to be reported elsewhere) that document Pcbp2 binding to a pyrimidine-rich tract within the 5′ untranslated region of its own mRNA. This suggests a feedback inhibition of Pcbp2 on the translation of its mRNA. Importantly, we demonstrate that embryos homozygous for the Pcbp2-deleted allele have a complete loss of Pcbp2 protein (Fig. 1C).

Mice haploinsufficient for Pcbp1 or Pcbp2 protein expression demonstrate a postnatal weight gain defect. Growth impairment as determined by weight is a common finding in mouse gene knockout models and can reflect complex perturbations that are difficult to characterize mechanistically (77). Our studies of Pcbp-haploinsufficient mice failed to reveal evidence for prenatal intrauterine growth retardation and placental insufficiency (Fig. 3C) that might contribute to weight differences. The normal weights of the Pcbp1 and Pcbp2 heterozygotes were equivalent to those of wild-type littermates at weeks 1 and 2 for both genders, further supporting an etiology that selectively affected the mice in the early postnatal period. Importantly, the Pcbp1- and Pcbp2-haploinsufficient mice were grossly normal, were competent for reproduction, showed no physical defects or behavioral abnormalities, and were maintained for 16 months without evidence of excess mortality or decreased longevity. In contrast, compound haploinsufficiency in Pcbp1$^{+/em2}$ Pcbp2$^{+/-}$ mice resulted in fewer live-born pups than expected and a severely runted phenotype in the lone surviving female mouse (Fig. 3D and E). This suggests that haploinsufficiency for either Pcbp1 or Pcbp2 is partially compensated for by wild-type levels of the sister isoform. As Pcbp1 and Pcbp2 have similar ribonucleotide binding specificities and operate through direct interactions with target RNAs and RNA processing machinery core components (22, 25), we speculate that these findings are explained by a gene dose or dosage balance effect in pathways where Pcbp1 and Pcbp2 have overlapping functions (35, 62, 78). Thus, our data support a weight attenuation phenotype for Pcbp1- and Pcbp2-haploinsufficient and compound haploinsufficient mice, but at present the underlying specificity for this postnatal growth defect remains undetermined.

Absence of Pcbp2 results in midgestational demise characterized by abnormalities in the cardiovascular and hematopoietic compartments. The earliest evidence of cardiovascular compromise was observed at 12.5 dpc and consisted of variable degrees of subcutaneous edema and microhemorrhage. By 13.5 to 14.5 dpc, micro- and macrohemorrhage were evident throughout the embryo corpus, most notably in the trunk and neck. Coinciding with this observation, pericardial effusion and subcutaneous edema became more prominent by 13.5 dpc. Hemorrhage phenotypes associated with cardiovascular abnormalities at midgestation have been reported in numerous mouse knockout studies (79–81). While the etiology of this defect remains unclear in the present case, the gene ontology analysis of the transcriptome data indicated that upregulated transcripts in Pcbp2$^{-/-}$ fetal liver were enriched for genes important to vascular development, including *Wnt2*, *Emcn*, *Ntrk2*, *Efnb2*, *Sox17*, and *Cyr61* (see Table S2 in the supplemental material), and points to gene targets for further study.

Defects in the hematopoietic compartment were observed in Pcbp2$^{-/-}$ embryos. Delayed erythroid maturation and decreased mature erythroblast number in 12.5-dpc Pcbp2$^{-/-}$ fetal liver (Fig. 5A and B) indicate that normal fetal liver erythropoiesis depends upon Pcbp2 function. Prior studies in our laboratory have documented that a Pcbp complex integrates cotranscriptional controls over human α-globin transcript processing in the nucleus (splicing and 3′ cleavage/polyadenylation) with control over its stability in the cytoplasm to maintain high-level expression of human α-globin mRNA during erythroblast differentiation (20, 22, 26, 82–85). Transcriptome profiling revealed both a marked downregulation of α-globin (*Hba1*) mRNA and decrease in global erythroid gene expression in Pcbp2$^{-/-}$ fetal liver (Fig. 7C and E). Our previous and current data suggest that Pcbp2 impacts erythroid development through posttranscriptional regulation of mRNA fate in this lineage. In ongoing studies we will utilize erythroid-specific inactivation of Pcpb2 expression to further define these erythropoietic defects.

A second clear defect in the hematopoietic system was identified by the analysis of megakaryocytes in the Pcbp2-null embryos (Fig. 6). The absence of apparent defects in granulocyte and monocyte lineage cell number (data not shown) suggests that Pcbp2 loss has a greater impact upon the megakaryocyte-erythrocyte progenitor (MEP) cell population. Several transcription factors regulate MEP lineage determination (KLF1 and FLI1) and

maturation of erythrocytes and megakaryocytes (GATA1, TAL1, FOG1, NF-E2, and GFIIB) (86). We observed downregulation of Klf1, Tal1, and Nfe2 in Pcbp2$^{-/-}$ 12.5-dpc fetal liver, which decreased 42%, 46%, and 60%, respectively (Fig. 7C; see also Table S1 in the supplemental material). The importance of posttranscriptional control of GATA1 mRNA has been demonstrated during zebrafish erythropoiesis (87). Of note, GATA1 mRNA expression was downregulated 37% in our analysis, but expression changes did not reach statistical significance at our conservative threshold (adjusted *P* value of 0.009) (data not shown). Several microRNAs also have emerged as important regulators of MEP lineage commitment (88). These studies highlight the relevance of protein-RNA interactions and posttranscriptional regulatory networks in erythrocyte and megakaryocyte hematopoiesis. It remains unclear if the hemorrhage phenotype we observe in Pcbp2-null embryos is linked to abnormal megakaryopoiesis since mice with lineage-specific impairment of megakaryocyte differentiation resulting in thrombocytopenia survive to term with evidence of bleeding only occurring after birth (89). Therefore, the hemorrhage in Pcbp2-null embryos and the decrease in megakaryocyte population, although both significant observations, may be functionally unrelated.

Global transcriptome profiling in Pcbp2$^{-/-}$ fetal liver demonstrated significant abnormalities in hematopoietic gene expression. Pcbp2 gene deletion repressed transcriptional programs essential for erythroid, megakaryocyte, and myeloid differentiation, while hematopoietic stem cell and lymphoid gene signatures were spared (Fig. 7E and F). These data suggest that Pcbp2 function is an important determinant of gene expression in the common myeloid progenitor and descendant lineages. This hypothesis is compatible with the diminished numbers of mature erythroid and megakaryocytic cells we observed (Fig. 6 and 7). In contrast, mature neutrophil and monocyte cell numbers were not altered by Pcbp2 deletion (data not shown), suggesting that terminal differentiation in these lineages may recover from upstream gene expression changes attributable to Pcbp2 function. It remains unclear whether Pcbp2 alters the fetal liver transcriptome through control of key regulators or an aggregate impact of direct effects on a large subset of lineage-defining genes (an mRNP operon) (2). It is well understood that transcription factors critical for multipotent progenitor cell fate determination can also act as secondary fate determinants for specific downstream lineages. For example, C/EBPα is essential for both early hematopoietic progenitors and specification of granulocytic lineages (90). Additional evidence suggests that both the timing and dosage of myeloid transcription factors are independent and critical parameters required for normal myelopoiesis (for a review, see reference 91). Further experimentation with lineage-restricted Pcbp2 deletion will be needed to determine if the observed gene expression changes are dependent upon the timing of gene disruption or reflect critical steady-state Pcbp2 functions.

In summary, the present report reveals that both Pcbp2 and its retrotransposed paralog Pcbp1 are required for normal embryogenesis and mouse viability. The data further indicate that Pcbp1 and Pcbp2 play distinct and nonredundant roles in embryonic development. While Pcbp1$^{em2/em2}$ homozygosity results in an early embryonic lethality, Pcbp2$^{-/-}$ embryos display impaired erythrocyte and megakaryocyte hematopoiesis and midgestational demise characterized by severe hemorrhage and edema. These findings highlight a clear example of a retrotransposition event that resulted in the acquisition of a function(s) by the daughter gene that is essential for mammalian survival.

ACKNOWLEDGMENTS

We are grateful for productive discussions with members of the Liebhaber laboratory. We also thank Jerrold M. Ward and Histoserv, Inc., for help with the initial phases of this study.

This work was supported by NIH MERIT HL 65449 (S.A.L.), NIH Children's Health Research Career Development Award K12-HD04335 (L.R.G.), and core facilities of the NIH/NIDDK P30-DK050306 Center for Molecular Studies in Digestive and Liver Diseases (Molecular Pathology and Imaging, Molecular Biology/Gene Expression, Cell Culture, and Transgenic and Chimeric Mouse Cores).

We declare that we have no conflicts of interest.

FUNDING INFORMATION

HHS | NIH | National Heart, Lung, and Blood Institute (NHLBI) provided funding to Stephen A. Liebhaber under grant number MERIT HL 65449. HHS | NIH | National Institute of Child Health and Human Development (NICHD) provided funding to Louis R. Ghanem under grant number K12-HD04335.

REFERENCES

1. **Moore MJ, Proudfoot NJ.** 2009. Pre-mRNA processing reaches back to transcription and ahead to translation. Cell **136:**688–700. http://dx.doi.org/10.1016/j.cell.2009.02.001.
2. **Keene JD.** 2010. Minireview: global regulation and dynamics of ribonucleic Acid. Endocrinology **151:**1391–1397. http://dx.doi.org/10.1210/en.2009-1250.
3. **Tian Q, Nakayama T, Dixon MP, Christian JL.** 1999. Post-transcriptional regulation of Xwnt-8 expression is required for normal myogenesis during vertebrate embryonic development. Development **126:**3371–3380.
4. **Blech-Hermoni Y, Ladd AN.** 2013. RNA binding proteins in the regulation of heart development. Int J Biochem Cell Biol **45:**2467–2478. http://dx.doi.org/10.1016/j.biocel.2013.08.008.
5. **Kim B-M, Buchner G, Miletich I, Sharpe PT, Shivdasani RA.** 2005. The stomach mesenchymal transcription factor Barx1 specifies gastric epithelial identity through inhibition of transient Wnt signaling. Dev Cell **8:**611–622. http://dx.doi.org/10.1016/j.devcel.2005.01.015.
6. **Gorgoni B, Richardson WA, Burgess HM, Anderson RC, Wilkie GS, Gautier P, Martins JPS, Brook M, Sheets MD, Gray NK.** 2011. Poly(A)-binding proteins are functionally distinct and have essential roles during vertebrate development. Proc Natl Acad Sci U S A **108:**7844–7849. http://dx.doi.org/10.1073/pnas.1017664108.
7. **Yang J, Chan CY, Jiang B, Yu X, Zhu G-Z, Chen Y, Barnard J, Mei W.** 2009. hnRNP I inhibits Notch signaling and regulates intestinal epithelial homeostasis in the zebrafish. PLoS Genet **5:**e1000363. http://dx.doi.org/10.1371/journal.pgen.1000363.
8. **Takahashi T, Suzuki H, Imai T, Shibata S, Tabuchi Y, Tsuchimoto K, Okano H, Hibi T.** 2013. Musashi-1 post-transcriptionally enhances phosphotyrosine-binding domain-containing m-Numb protein expression in regenerating gastric mucosa. PLoS One **8:**e53540. http://dx.doi.org/10.1371/journal.pone.0053540.
9. **Guallar D, Wang J.** 2014. RNA-binding proteins in pluripotency, differentiation, and reprogramming. Front Biol (Beijing) **9:**389–409. http://dx.doi.org/10.1007/s11515-014-1326-y.
10. **Mueller AA, Cheung TH, Rando TA.** 2013. All's well that ends well: alternative polyadenylation and its implications for stem cell biology. Curr Opin Cell Biol **25:**222–232. http://dx.doi.org/10.1016/j.ceb.2012.12.008.
11. **Kini HK, Kong J, Liebhaber SA.** 2014. Cytoplasmic poly(A) binding protein C4 serves a critical role in erythroid differentiation. Mol Cell Biol **34:**1300–1309. http://dx.doi.org/10.1128/MCB.01683-13.
12. **Ostareck DH, Ostareck-Lederer A, Wilm M, Thiele BJ, Mann M, Hentze MW.** 1997. mRNA silencing in erythroid differentiation: hnRNP K and hnRNP E1 regulate 15-lipoxygenase translation from the 3′ end. Cell **89:**597–606. http://dx.doi.org/10.1016/S0092-8674(00)80241-X.
13. **Williamson AJK, Smith DL, Blinco D, Unwin RD, Pearson S, Wilson C, Miller C, Lancashire L, Lacaud G, Kouskoff V, Whetton AD.** 2008. Quantitative proteomics analysis demonstrates post-transcriptional regu-

lation of embryonic stem cell differentiation to hematopoiesis. Mol Cell Proteomics **7:**459–472.
14. **Ostareck-Lederer A, Ostareck DH.** 2004. Control of mRNA translation and stability in haematopoietic cells: the function of hnRNPs K and E1/E2. Biol Cell **96:**407–411. http://dx.doi.org/10.1016/j.biolcel.2004.03.010.
15. **Makeyev AV, Liebhaber SA.** 2002. The poly(C)-binding proteins: a multiplicity of functions and a search for mechanisms. RNA **8:**265–278. http://dx.doi.org/10.1017/S1355838202024627.
16. **Makeyev AV, Chkheidze AN, Liebhaber SA.** 1999. A set of highly conserved RNA-binding proteins, alphaCP-1 and alphaCP-2, implicated in mRNA stabilization, are coexpressed from an intronless gene and its intron-containing paralog. J Biol Chem **274:**24849–24857. http://dx.doi.org/10.1074/jbc.274.35.24849.
17. **Aasheim HC, Loukianova T, Deggerdal A, Smeland EB.** 1994. Tissue specific expression and cDNA structure of a human transcript encoding a nucleic acid binding [oligo(dC)] protein related to the pre-mRNA binding protein K. Nucleic Acids Res **22:**959–964. http://dx.doi.org/10.1093/nar/22.6.959.
18. **Leffers H, Dejgaard K, Celis JE.** 1995. Characterisation of two major cellular poly(rC)-binding human proteins, each containing three K-homologous (KH) domains. Eur J Biochem **230:**447–453. http://dx.doi.org/10.1111/j.1432-1033.1995.tb20581.x.
19. **Chaudhury A, Chander P, Howe PH.** 2010. Heterogeneous nuclear ribonucleoproteins (hnRNPs) in cellular processes: Focus on hnRNP E1's multifunctional regulatory roles. RNA **16:**1449–1462. http://dx.doi.org/10.1261/rna.2254110.
20. **Waggoner SA, Liebhaber SA.** 2003. Identification of mRNAs associated with αCP2-containing RNP complexes. Mol Cell Biol **23:**7055–7067. http://dx.doi.org/10.1128/MCB.23.19.7055-7067.2003.
21. **Flynn RA, Martin L, Spitale RC, Do BT, Sagan SM, Zarnegar B, Qu K, Khavari PA, Quake SR, Sarnow P, Chang HY.** 2015. Dissecting noncoding and pathogen RNA-protein interactomes. RNA **21:**135–143. http://dx.doi.org/10.1261/rna.047803.114.
22. **Ji X, Kong J, Liebhaber SA.** 2011. An RNA-protein complex links enhanced nuclear 3′ processing with cytoplasmic mRNA stabilization. EMBO J **30:**2622–2633. http://dx.doi.org/10.1038/emboj.2011.171.
23. **Ji X, Kong J, Carstens RP, Liebhaber SA.** 2007. The 3′ untranslated region complex involved in stabilization of human alpha-globin mRNA assembles in the nucleus and serves an independent role as a splice enhancer. Mol Cell Biol **27:**3290–3302. http://dx.doi.org/10.1128/MCB.02289-05.
24. **Thisted T, Lyakhov DL, Liebhaber SA.** 2001. Optimized RNA targets of two closely related triple KH domain proteins, heterogeneous nuclear ribonucleoprotein K and αCP-2KL, suggest distinct modes of RNA recognition. J Biol Chem **276:**17484–17496. http://dx.doi.org/10.1074/jbc.M010594200.
25. **Makeyev AV, Eastmond DL, Liebhaber SA.** 2002. Targeting a KH-domain protein with RNA decoys. RNA **8:**1160–1173. http://dx.doi.org/10.1017/S135583820202808X.
26. **Ji X, Wan J, Vishnu M, Xing Y, Liebhaber SA.** 2013. αCP poly(C) binding proteins act as global regulators of alternative polyadenylation. Mol Cell Biol **33:**2560–2573. http://dx.doi.org/10.1128/MCB.01380-12.
27. **Wu C, Orozco C, Boyer J, Leglise M, Goodale J, Batalov S, Hodge CL, Haase J, Janes J, Huss JW, Su AI.** 2009. BioGPS: an extensible and customizable portal for querying and organizing gene annotation resources. Genome Biol **10:**R130. http://dx.doi.org/10.1186/gb-2009-10-11-r130.
28. **Geng C, Macdonald PM.** 2007. Identification of genes that influence gurken expression. Fly **1:**259–267. http://dx.doi.org/10.4161/fly.5246.
29. **Charroux B, Angelats C, Fasano L, Kerridge S, Vola C.** 1999. The levels of the *bancal* product, a *Drosophila* homologue of vertebrate hnRNP K protein, affect cell proliferation and apoptosis in imaginal disc cells. Mol Cell Biol **19:**7846–7856. http://dx.doi.org/10.1128/MCB.19.11.7846.
30. **Colaiácovo MP, Stanfield GM, Reddy KC, Reinke V, Kim SK, Villeneuve AM.** 2002. A targeted RNAi screen for genes involved in chromosome morphogenesis and nuclear organization in the *Caenorhabditis elegans* germline. Genetics **162:**113–128.
31. **Roshon MJ, Ruley HE.** 2005. Hypomorphic mutation in hnRNP U results in post-implantation lethality. Transgenic Res **14:**179–192. http://dx.doi.org/10.1007/s11248-004-8147-8.
32. **Williamson DJ, Banik-Maiti S, DeGregori J, Ruley HE.** 2000. hnRNP C is required for postimplantation mouse development but Is dispensable for cell viability. Mol Cell Biol **20:**4094–4105. http://dx.doi.org/10.1128/MCB.20.11.4094-4105.2000.
33. **Katsanou V, Milatos S, Yiakouvaki A, Sgantzis N, Kotsoni A, Alexiou M, Harokopos V, Aidinis V, Hemberger M, Kontoyiannis DL.** 2009. The RNA-binding protein Elavl1/HuR is essential for placental branching morphogenesis and embryonic development. Mol Cell Biol **29:**2762–2776. http://dx.doi.org/10.1128/MCB.01393-08.
34. **Shibayama M, Ohno S, Osaka T, Sakamoto R, Tokunaga A, Nakatake Y, Sato M, Yoshida N.** 2009. Polypyrimidine tract-binding protein is essential for early mouse development and embryonic stem cell proliferation. FEBS J **276:**6658–6668. http://dx.doi.org/10.1111/j.1742-4658.2009.07380.x.
35. **Waggoner SA, Johannes GJ, Liebhaber SA.** 2009. Depletion of the poly(C)-binding proteins αCP1 and αCP2 from K562 cells leads to p53-independent induction of cyclin-dependent kinase inhibitor (CDKN1A) and G1 arrest. J Biol Chem **284:**9039–9049. http://dx.doi.org/10.1074/jbc.M806986200.
36. **Gamarnik AV, Andino R.** 1997. Two functional complexes formed by KH domain containing proteins with the 5′ noncoding region of poliovirus RNA. RNA **3:**882–892.
37. **Tang Y-S, Khan RA, Zhang Y, Xiao S, Wang M, Hansen DK, Jayaram HN, Antony AC.** 2011. Incrimination of heterogeneous nuclear ribonucleoprotein E1 (hnRNP-E1) as a candidate sensor of physiological folate deficiency. J Biol Chem **286:**39100–39115. http://dx.doi.org/10.1074/jbc.M111.230938.
38. **Shi H, Bencze KZ, Stemmler TL, Philpott CC.** 2008. A cytosolic iron chaperone that delivers iron to ferritin. Science **320:**1207–1210. http://dx.doi.org/10.1126/science.1157643.
39. **Blyn LB, Towner JS, Semler BL, Ehrenfeld E.** 1997. Requirement of poly(rC) binding protein 2 for translation of poliovirus RNA. J Virol **71:**6243–6246.
40. **Perrotti D, Calabretta B.** 2002. Post-transcriptional mechanisms in BCR/ABL leukemogenesis: role of shuttling RNA-binding proteins. Oncogene **21:**8577–8583. http://dx.doi.org/10.1038/sj.onc.1206085.
41. **Woolaway K, Asai K, Emili A, Cochrane A.** 2007. hnRNP E1 and E2 have distinct roles in modulating HIV-1 gene expression. Retrovirology **4:**28. http://dx.doi.org/10.1186/1742-4690-4-28.
42. **Chaudhury A, Hussey GS, Ray PS, Jin G, Fox PL, Howe PH.** 2010. TGF-β-mediated phosphorylation of hnRNP E1 induces EMT via transcript-selective translational induction of Dab2 and ILEI. Nat Cell Biol **12:**286–293. http://dx.doi.org/10.1038/ncb2029.
43. **Hussey GS, Chaudhury A, Dawson AE, Lindner DJ, Knudsen CR, Wilce MCJ, Merrick WC, Howe PH.** 2011. Identification of an mRNP complex regulating tumorigenesis at the translational elongation step. Mol Cell **41:**419–431. http://dx.doi.org/10.1016/j.molcel.2011.02.003.
44. **Ghanem LR, Chatterji P, Liebhaber SA.** 2014. Specific enrichment of the RNA-binding proteins PCBP1 and PCBP2 in chief cells of the murine gastric mucosa. Gene Expr Patterns **14:**78–87. http://dx.doi.org/10.1016/j.gep.2014.01.004.
45. **Ye J, Coulouris G, Zaretskaya I, Cutcutache I, Rozen S, Madden TL.** 2012. Primer-BLAST: a tool to design target-specific primers for polymerase chain reaction. BMC Bioinformatics **13:**134. http://dx.doi.org/10.1186/1471-2105-13-134.
46. **Rotmistrovsky K, Jang W, Schuler GD.** 2004. A web server for performing electronic PCR. Nucleic Acids Res **32:**W108–W112. http://dx.doi.org/10.1093/nar/gkh450.
47. **Miller JC, Tan S, Qiao G, Barlow KA, Wang J, Xia DF, Meng X, Paschon DE, Leung E, Hinkley SJ, Dulay GP, Hua KL, Ankoudinova I, Cost GJ, Urnov FD, Zhang HS, Holmes MC, Zhang L, Gregory PD, Rebar EJ.** 2011. A TALE nuclease architecture for efficient genome editing. Nat Biotechnol **29:**143–148. http://dx.doi.org/10.1038/nbt.1755.
48. **Liu P, Jenkins NA, Copeland NG.** 2003. A highly efficient recombineering-based method for generating conditional knockout mutations. Genome Res **13:**476–484. http://dx.doi.org/10.1101/gr.749203.
49. **Eggan K, Akutsu H, Loring J, Jackson-Grusby L, Klemm M, Rideout WM, Yanagimachi R, Jaenisch R.** 2001. Hybrid vigor, fetal overgrowth, and viability of mice derived by nuclear cloning and tetraploid embryo complementation. Proc Natl Acad Sci U S A **98:**6209–6214. http://dx.doi.org/10.1073/pnas.101118898.
50. **Nagy A, Gertsenstein M, Vintersten K, Behringer R.** 2003. Manipulating the mouse embryo, 3rd ed. Cold Spring Harbor Laboratory Press, Cold Spring Harbor, NY.
51. **Koulnis M, Pop R, Porpiglia E, Shearstone JR, Hidalgo D, Socolovsky**

M. 2011. Identification and analysis of mouse erythroid progenitors using the CD71/TER119 flow-cytometric assay. J Vis Exp **5:**2809.
52. **Shearstone JR, Pop R, Bock C, Boyle P, Meissner A, Socolovsky M.** 2011. Global DNA demethylation during mouse erythropoiesis in vivo. Science **334:**799–802. http://dx.doi.org/10.1126/science.1207306.
53. **Camacho C, Coulouris G, Avagyan V, Ma N, Papadopoulos J, Bealer K, Madden TL.** 2009. BLAST+: architecture and applications. BMC Bioinformatics **10:**421. http://dx.doi.org/10.1186/1471-2105-10-421.
54. **Trapnell C, Pachter L, Salzberg SL.** 2009. TopHat: discovering splice junctions with RNA-Seq. Bioinformatics **25:**1105–1111. http://dx.doi.org/10.1093/bioinformatics/btp120.
55. **Anders S, Pyl PT, Huber W.** 2015. HTSeq—a Python framework to work with high-throughput sequencing data. Bioinformatics **31:**166–169. http://dx.doi.org/10.1093/bioinformatics/btu638.
56. **Martin M.** 2011. Cutadapt removes adapter sequences from high-throughput sequencing reads. EMBnet J **17:**10–12. http://dx.doi.org/10.14806/ej.17.1.200.
57. **Love MI, Huber W, Anders S.** 2014. Moderated estimation of fold change and dispersion for RNA-seq data with DESeq2. Genome Biol **15:**550. http://dx.doi.org/10.1186/s13059-014-0550-8.
58. **D'Alton S, Altshuler M, Lewis J.** 2015. Studies of alternative isoforms provide insight into TDP-43 autoregulation and pathogenesis. RNA **21:**1419–1432. http://dx.doi.org/10.1261/rna.047647.114.
59. **Hornstein E, Git A, Braunstein I, Avni D, Meyuhas O.** 1999. The expression of poly(A)-binding protein gene is translationally regulated in a growth-dependent fashion through a 5′-terminal oligopyrimidine tract motif. J Biol Chem **274:**1708–1714. http://dx.doi.org/10.1074/jbc.274.3.1708.
60. **Tesson L, Usal C, Ménoret S, Leung E, Niles BJ, Remy S, Santiago Y, Vincent AI, Meng X, Zhang L, Gregory PD, Anegon I, Cost GJ.** 2011. Knockout rats generated by embryo microinjection of TALENs. Nat Biotechnol **29:**695–696. http://dx.doi.org/10.1038/nbt.1940.
61. **Sanjana NE, Cong L, Zhou Y, Cunniff MM, Feng G, Zhang F.** 2012. A transcription activator-like effector toolbox for genome engineering. Nat Protoc **7:**171–192. http://dx.doi.org/10.1038/nprot.2011.431.
62. **Qian W, Zhang J.** 2008. Gene dosage and gene duplicability. Genetics **179:**2319–2324. http://dx.doi.org/10.1534/genetics.108.090936.
63. **Kong J, Sumaroka M, Eastmond DL, Liebhaber SA.** 2006. Shared stabilization functions of pyrimidine-rich determinants in the erythroid 15-lipoxygenase and alpha-globin mRNAs. Mol Cell Biol **26:**5603–5614. http://dx.doi.org/10.1128/MCB.01845-05.
64. **Palis J, Robertson S, Kennedy M, Wall C, Keller G.** 1999. Development of erythroid and myeloid progenitors in the yolk sac and embryo proper of the mouse. Development **126:**5073–5084.
65. **Vannucchi AM, Paoletti F, Linari S, Cellai C, Caporale R, Ferrini PR, Sanchez M, Migliaccio G, Migliaccio AR.** 2000. Identification and characterization of a bipotent (erythroid and megakaryocytic) cell precursor from the spleen of phenylhydrazine-treated mice. Blood **95:**2559–2568.
66. **Akashi K, Traver D, Miyamoto T, Weissman IL.** 2000. A clonogenic common myeloid progenitor that gives rise to all myeloid lineages. Nature **404:**193–197. http://dx.doi.org/10.1038/35004599.
67. **Huang DW, Sherman BT, Lempicki RA.** 2009. Systematic and integrative analysis of large gene lists using DAVID bioinformatics resources. Nat Protoc **4:**44–57. http://dx.doi.org/10.1038/nprot.2008.211.
68. **Novershtern N, Subramanian A, Lawton LN, Mak RH, Haining WN, McConkey ME, Habib N, Yosef N, Chang CY, Shay T, Frampton GM, Drake ACB, Leskov I, Nilsson B, Preffer F, Dombkowski D, Evans JW, Liefeld T, Smutko JS, Chen J, Friedman N, Young RA, Golub TR, Regev A, Ebert BL.** 2011. Densely interconnected transcriptional circuits control cell states in human hematopoiesis. Cell **144:**296–309. http://dx.doi.org/10.1016/j.cell.2011.01.004.
69. **Pimkin M, Kossenkov AV, Mishra T, Morrissey CS, Wu W, Keller CA, Blobel GA, Lee D, Beer MA, Hardison RC, Weiss MJ.** 2014. Divergent functions of hematopoietic transcription factors in lineage priming and differentiation during erythro-megakaryopoiesis. Genome Res **24:**1932–1944. http://dx.doi.org/10.1101/gr.164178.113.
70. **Ho JJD, Robb GB, Tai SC, Turgeon PJ, Mawji IA, Man HSJ, Marsden PA.** 2013. Active stabilization of human endothelial nitric oxide synthase mRNA by hnRNP E1 protects against antisense RNA and microRNAs. Mol Cell Biol **33:**2029–2046. http://dx.doi.org/10.1128/MCB.01257-12.
71. **Makeyev AV, Liebhaber SA.** 2000. Identification of two novel mammalian genes establishes a subfamily of KH-domain RNA-binding proteins. Genomics **67:**301–316. http://dx.doi.org/10.1006/geno.2000.6244.
72. **Valverde R, Edwards L, Regan L.** 2008. Structure and function of KH domains. FEBS J **275:**2712–2726. http://dx.doi.org/10.1111/j.1742-4658.2008.06411.x.
73. **Lunde BM, Moore C, Varani G.** 2007. RNA-binding proteins: modular design for efficient function. Nat Rev Mol Cell Biol **8:**479–490. http://dx.doi.org/10.1038/nrm2178.
74. **Feng Y, Absher D, Eberhart DE, Brown V, Malter HE, Warren ST.** 1997. FMRP associates with polyribosomes as an mRNP, and the I304N mutation of severe fragile X syndrome abolishes this association. Mol Cell **1:**109–118. http://dx.doi.org/10.1016/S1097-2765(00)80012-X.
75. **Maquat LE, Li X.** 2001. Mammalian heat shock p70 and histone H4 transcripts, which derive from naturally intronless genes, are immune to nonsense-mediated decay. RNA **7:**445–456. http://dx.doi.org/10.1017/S1355838201002229.
76. **Neu-Yilik G, Gehring NH, Thermann R, Frede U, Hentze MW, Kulozik AE.** 2001. Splicing and 3′ end formation in the definition of nonsense-mediated decay-competent human beta-globin mRNPs. EMBO J **20:**532–540. http://dx.doi.org/10.1093/emboj/20.3.532.
77. **Reed DR, Lawler MP, Tordoff MG.** 2008. Reduced body weight is a common effect of gene knockout in mice. BMC Genet **9:**4. http://dx.doi.org/10.1186/1471-2156-9-4.
78. **Deutschbauer AM, Jaramillo DF, Proctor M, Kumm J, Hillenmeyer ME, Davis RW, Nislow C, Giaever G.** 2005. Mechanisms of haploinsufficiency revealed by genome-wide profiling in yeast. Genetics **169:**1915–1925. http://dx.doi.org/10.1534/genetics.104.036871.
79. **Park T-J, Boyd K, Curran T.** 2006. Cardiovascular and craniofacial defects in Crk-null mice. Mol Cell Biol **26:**6272–6282. http://dx.doi.org/10.1128/MCB.00472-06.
80. **Arthur J, Elce JS, Hegadorn C, Williams K, Greer PA.** 2000. Disruption of the murine calpain small subunit gene, Capn4: calpain is essential for embryonic development but not for cell growth and division. Mol Cell Biol **20:**4474–4481. http://dx.doi.org/10.1128/MCB.20.12.4474-4481.2000.
81. **Hisa T, Spence SE, Rachel RA, Fujita M, Nakamura T, Ward JM, Devor-Henneman DE, Saiki Y, Kutsuna H, Tessarollo L, Jenkins NA, Copeland NG.** 2004. Hematopoietic, angiogenic and eye defects in Meis1 mutant animals. EMBO J **23:**450–459. http://dx.doi.org/10.1038/sj.emboj.7600038.
82. **Ji X, Kong J, Liebhaber SA.** 2003. In vivo association of the stability control protein αCP with actively translating mRNAs. Mol Cell Biol **23:**899–907. http://dx.doi.org/10.1128/MCB.23.3.899-907.2003.
83. **Kong J, Ji X, Liebhaber SA.** 2003. The KH-domain protein αCP has a direct role in mRNA stabilization independent of its cognate binding site. Mol Cell Biol **23:**1125–1134. http://dx.doi.org/10.1128/MCB.23.4.1125-1134.2003.
84. **Kong J, Liebhaber SA.** 2007. A cell type-restricted mRNA surveillance pathway triggered by ribosome extension into the 3′ untranslated region. Nat Struct Mol Biol **14:**670–676. http://dx.doi.org/10.1038/nsmb1256.
85. **Weiss IM, Liebhaber SA.** 1994. Erythroid cell-specific determinants of alpha-globin mRNA stability. Mol Cell Biol **14:**8123–8132. http://dx.doi.org/10.1128/MCB.14.12.8123.
86. **Crispino JD, Weiss MJ.** 2014. Erythro-megakaryocytic transcription factors associated with hereditary anemia. Blood **123:**3080–3088. http://dx.doi.org/10.1182/blood-2014-01-453167.
87. **Li X, Lu Y-C, Dai K, Torregroza I, Hla T, Evans T.** 2014. Elavl1a regulates zebrafish erythropoiesis via posttranscriptional control of gata1. Blood **123:**1384–1392. http://dx.doi.org/10.1182/blood-2013-09-526962.
88. **Zhang L, Sankaran VG, Lodish HF.** 2012. MicroRNAs in erythroid and megakaryocytic differentiation and megakaryocyte-erythroid progenitor lineage commitment. Leukemia **26:**2310–2316. http://dx.doi.org/10.1038/leu.2012.137.
89. **Shivdasani RA, Rosenblatt MF, Zucker-Franklin D, Jackson CW, Hunt P, Saris CJ, Orkin SH.** 1995. Transcription factor NF-E2 is required for platelet formation independent of the actions of thrombopoietin/MGDF in megakaryocyte development. Cell **81:**695–704. http://dx.doi.org/10.1016/0092-8674(95)90531-6.
90. **Iwasaki H, Mizuno S, Arinobu Y, Ozawa H, Mori Y, Shigematsu H, Takatsu K, Tenen DG, Akashi K.** 2006. The order of expression of transcription factors directs hierarchical specification of hematopoietic lineages. Genes Dev **20:**3010–3021. http://dx.doi.org/10.1101/gad.1493506.
91. **Iwasaki H, Akashi K.** 2007. Myeloid lineage commitment from the hematopoietic stem cell. Immunity **26:**726–740. http://dx.doi.org/10.1016/j.immuni.2007.06.004.